LONGITUDINAL ANALYSIS OF PATIENTS WITH MILD TRAUMATIC BRAIN INJURY ASSESSED WITH REGIONAL VOLUMES AND DTI PARAMETERS

by
Zhongyan Xiong

A dissertation submitted to Johns Hopkins University in conformity with the requirements for the degree of Master of Science

Baltimore, Maryland
May 2020

Abstract

Traumatic brain injury (TBI) is a serious public health problem in the United States, and mild TBI is the most common type of TBI. It is associated with brain volume loss and axonal injury. Diffusion-weighted imaging (DWI) is an imaging method sensitive to white matter changes that is used to study the diffusion pattern of water molecules and show the microstructures of axonal tissues. In this study, regional changes in mild TBI patients and healthy controls are evaluated and compared using both high-resolution T1-weighted imaging and DWI. Seventy-six mild TBI patients were imaged in four visits after injury: within ten days, after one month, after six months, and after 18 months. Fifty-one healthy controls were imaged in two visits with a six-month interval. In volumetric analysis, it was hypothesized that mild TBI patients would show a decrease in WM and GM volumes while an increase in CSF volume compared with healthy controls over time. Analyses from the

ABSTRACT

multi-atlas based segmented brain images reveal that no significant results were found in GM, WM, and CSF. However, six areas of GM were found to have significant differences between the mTBI group and healthy controls. The trends agree with the hypothesis that gray matter volume would decrease while CSF volume would increase longitudinally in mild TBI patients. In the longitudinal study of volume comparison, another six gray matter regions and three ventricle regions were found to have significant changes over time for mTBI patients. In DTI metrics analysis, it was hypothesized that mild TBI patients would show decreased fractional anisotropy (FA), mean diffusivity (MD), decreased axial diffusivity (AD), and radial diffusivity (RD) compared to healthy controls over time. However, in this study, analyses of FA, MD, AD, and RD from the DTI images do not show significant diffusion changes over time in patients compared to healthy controls.

Primary Reader and Advisor: Jerry L. Prince

Secondary Reader: Matthew E. Peters

Acknowledgments

I am very grateful to my advisor, Professor Jerry Prince, for all the instructions and guidance. I am thankful to him for always being patient and for encouraging me to explore different research ideas and conduct research through trial and error, which not only helped me to shape my independent research interests but also made the research process enjoyable. In the process of writing and revision my thesis, he went through all the stages of the writing of this thesis and checked all the details for ensuring the quality. I have learned a lot from him on the importance of precise and rigorous writing in scientific papers and reports. Without his consistent and illuminating instruction, this thesis could not have reached its present form.

I am also grateful to Professor Matthew Peters for always being supportive in my thesis. He has provided many profound advices on what I did and what to do. I would also like to express my gratitude to my family and friends for their loving considerations and great confidence in me through my master years.

Contents

List of Tables

List of Figures

Chapter 1 Introduction

A traumatic brain injury (TBI) is defined as a blow to the head or a penetrating head injury that disrupts the normal function of the brain [1]. TBI is a serious public health problem in the United States [2], causing a large number of deaths and permanent disability each year. Approximately 2.5 million TBI-related emergency department visits were made in the United States in 2014 [3]. They were mostly due to motor-vehicle crashes (with over 72% of hospitalizations), unintentional falls, and assaults. Rates of TBI related emergency department visits increased from 2006 to 2014 and the trend continues [4]. When getting a TBI, a loss of consciousness and confusion and disorientation can occur [5]. If the symptoms stop within 30 minutes, the level of severity is considered to be mild; otherwise, it is considered to be moderate or severe TBI [6]. Mild TBI is the most common type of TBI [1]. Children and elders are at a high risk for mild TBI, with a

rate of 2,232 out of 100,000 in adults older than 75 years and a rate of 1,592 out of 100,000 in children younger than 5 years old [37]. The symptoms of mild TBI includes cognitive problems like headaches, emotionality, and depression [8]. Patients often find difficulty in thinking, memorizing, and paying attention [8]. Since the symptoms are mild, the patients look normal and move as usual, and the diagnosis might be missed.

The Glasgow Coma Score (GCS) is a scoring system to estimate coma severity according to criteria from different areas of brain function including visual, verbal, and motor function [9]. The range of GCS is from 3 to 15 and it is commonly used to estimate TBI severity [9]. The lower the value, the more severe the disease and more likely that the patient is in a coma state. For mild TBI patients, the GCS score is at the range of 13–15 [9].

There are several neuroimaging techniques used for mild TBI evaluation in MRI since MRI has good contrast in soft tissue and provides anatomy, structure, function, physiology, and metabolism information. White matter pathways, which includes the corona radiata (CR), internal capsule (IC), cerebral peduncle (CP), and corpus callosum (CC) are especially vulnerable to stretching and shearing [10]. MRI-based techniques used to evaluate white matter injury in mild TBI include diffusion-weighted imaging (DWI), magnetization transfer ratio (MTR), susceptibility weighted imaging (SWI) [10]. Among all these techniques, DWI is the most preferred modality.

The goal of the current study was to characterize the longitudinal structural changes in the brain (especially white matter, gray matter, and ventricle areas) over the 18 months after the injury and to characterize the cross-sectional difference between mild TBI patients and healthy controls. Since white matter is a likely candidate for the bulk of volume loss [11], diffusion metrics in white matter tracts were examined in addition to regional volumes. T1-weighted MP-RAGE and DWI images were used for volumetric comparison in brain and diffusion metric comparison in white matter tracts, respectively. It was hypothesized that mild TBI patients would show a decrease in white matter volume as well as FA decrease and MD increase over time. As for the gray matter, a decrease in volume was hypothesized.

Chapter 2 Literature review

Previous studies have investigated both longitudinal changes in TBI patients of different severities and differences between TBI patients and healthy controls. Table 1 shows a literature summary of important studies.

Table 1. Literature summary of longitudinal study of TBI patients.

	subjects	**Follow-up time**	**ROIs**	**Metrics**	**Type of study**	**results**
Sidaros et al. (2008) [11]	30 adult patients recovering from severe TBI and 30 healthy controls	8 weeks and 12 months post-injury	internal capsule and in centrum semiovale	FA, AD and RD	Longitudinal and cross-sectional	Fractional anisotropy was reduced, decreased AD, increased RD than HC; FA in patients had increased in the internal capsule and in centrum semiovale due to interval increase of AD with unchanged RD.
Bendlin et al. (2008) [13]	35 patients with moderate & severer TBI and 36 healthy controls	2 months and 12.7 months post-injury	corpus callosum, cingulum, the superior and inferior longitudinal fascicules, the uncinate fasciculus, and brain stem fiber tracts;	Volume; FA and MD	Longitudinal and cross-sectional	Deleterious GM and WM volume changes and decreased FA and increased MD over time in TBI patients compared to controls over large regions of the brain.

	subjects	Follow-up time	ROIs	Metrics	Type of study	results
Betz et al. (2012) [14]	59 patients with all different severity TBI	/	whole brain white matter, internal capsule, genu, splenium, and body of the corpus callosum	ADC, FA, AD and RD	Cross-sectional	DTI parameters at the whole-brain level and regional level can provide prognostic information about the discharge status of a patient; AD appears to provide the most prognostic information about outcome status, on both regional and global scales.
Zhou et al. (2013) [15]	28 mild TBI patients and 22 healthy controls	1-year post-injury	GM and WM	volume	Longitudinal and cross-sectional	Global atrophy in patients compared to controls; anterior Cingulate WM bilaterally and the left cingulate gyrus isthmus WM, as well as the right precuneal GM have longitudinally decrease
Stokum et al. (2015) [16]	24 mild TBI patients	ten days, one month and six months post-injury	thalamus, internal capsule, and corpus callosum	FA, MD, RD, mean kurtosis (MK) and radial kurtosis (Kr)	longitudinal	Reduced Kr and MK in the anterior internal capsule, reduced MK in the posterior internal capsule

Zhou et al. [17] examined longitudinal regional brain volume changes in mild TBI patients. Their data includes two visits with 1-year intervals of 28 patients and 22 matched control subjects. Global atrophy in brain volumes of patients were found. The anterior cingulate white matter (WM) bilaterally and the left cingulate gyrus isthmus WM as well as the right precuneal gray matter (GM) show longitudinal decreases. Anderson [18][19], Bigler [20], Gale [21], and Yount [22] examined volume changes of the corpus callosum, the cingulate gyrus, the hippocampus, the thalamus, and the fornix in TBI patients. They found moderate and severe TBI have demonstrated brain atrophy in those areas.

Bendlin [13] found deleterious GM and WM volume changes and

decreased FA and increased MD over time in DTI images of TBI patients compared to controls over large regions of the brain. He concluded that DTI measures may be more useful than high-resolution anatomical images in assessment of group differences.

Besides diffusion images, other imaging techniques have been used for longitudinal study of mild TBI patients, including proton spectroscopy and functional magnetic resonance (MR) imaging, which can show post-concussive microstructural, metabolic, and functional changes in the brain [15][23][24].

Chapter 2 Background

2.1 Magnetic resonance imaging

Magnetic resonance imaging (MRI) is a medical imaging technique used in radiology to form images of the anatomy [25]. MRI scanners use strong magnetic fields, magnetic field gradients, and radio waves to generate images of the organs in the body. An MR system is composed of a magnet, coils, and a computer system [26]. The magnet is used to generate the static magnetic field. The coils include shim coils (to make the magnetic field as equally distributed as possible), an RF coil (for Faraday induction in the body), a receiver coil (to detect the returning radio signals), and gradient coils (to provide spatial localization of the signals) [26]. The computer system is used for generation of pulse sequences and reconstruction of images from the

received signals [26].

Hydrogen nuclei contain protons with a nuclear magnetic spin property; they exist in every human cell. When a patient is placed within a magnetic field, these protons align like tiny magnets [27]. Radio frequency (RF) pulses produce an electromagnetic field that, when transmitted in a plane perpendicular to the magnet, excite the hydrogen protons. Radiofrequency energy is produced as the protons relax back to their original state, and this energy can then be received and reconstructed into images [28].

MRI can discriminate between tissues based on their physical properties. MRI is particularly useful at providing highly detailed images of soft tissues [26]. MRI scanning can also provide images in various planes without the movement of the patient.

The tissue contrast on an MR image can be manipulated by changing the pulse sequence parameters. A pulse sequence sets the specific number, strength, and timing of the RF and gradient pulses. The two most important parameters are the repetition time (TR) and the echo time (TE). The TR is the time between consecutive RF pulses. TE is the time between the initial RF pulse and the received signal peak (echo).

The most common pulse sequences are the T1-weighted and T2-weighted pulse sequences. On an MRI scan, some tissues appear to be brighter or darker than others. Brightness depends partly on the density of protons in that

area (higher density being associated with a brighter area). Brightness also depends on longitudinal relaxation time, known as T1, and transverse relaxation time, known as T2, of tissues. All of these properties are routinely used to show contrast between different soft tissues. A T1-weighted sequence uses a short TR and short TE (TR < 1000 ms, TE < 30 ms) [26]. A T2-weighted sequence uses a long TR and long TE (TR > 2000 ms, TE > 80 ms) [26]. The images produced by T1-weighted and T2-weighted sequences are called T1-weighted and T2-weighted images, respectively.

2.2 MP-RAGE

The three-dimension magnetization-prepared rapid gradient echo (MP-RAGE) sequence is one of the most popular sequences for high-resolution whole brain T1-weighted imaging [29]. It was first proposed by Muger and Brookeman [30]. MP-RAGE consists of a non-selective (180º) inversion pulse followed by a collection of rapidly acquired gradient echoes obtained at short TE's (2–4 ms) and small flip angles α (5–12º) [31]. A moderate inversion time (TI) of 600–900 ms and long repetition time (TR) of approximately 2000 ms are typical for MP-RAGE [31].

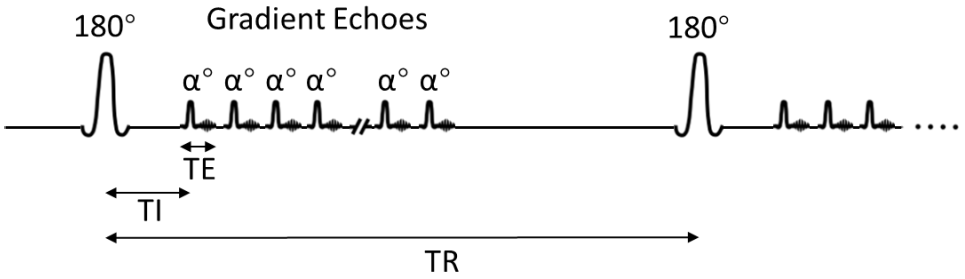

Figure 1. Schematic of the MP-RAGE sequence (imaging gradients omitted).

In most MP-RAGE acquisitions, the center of k-space is acquired shortly after the null point of cerebrospinal fluid (CSF), providing good contrast between CSF and other tissues as well as moderate contrast between WM and GM [32].

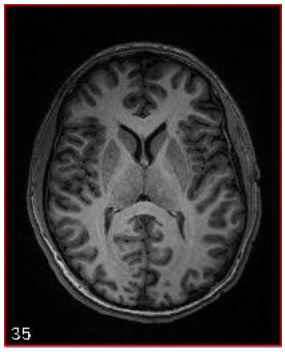

Figure 2. MP-RAGE brain image with TE = 3.44 ms, TR = 2250 ms, TI = 900 ms.

MP-RAGE images have been widely used for classifying brain tissues in voxel-based morphometry [33], detecting pathological changes of the brain [34], and estimating regional brain volume abnormalities associated with brain functions [35].

2.3 Diffusion Weighted Magnetic Resonance Imaging

Diffusion weighted magnetic resonance imaging (DWI) is a form of magnetic resonance imaging (MRI). DWI is presently the only tool for observing diffusion in vivo [25]. Water is the largest component in the human body and is found in both intra and extra cellular fluid. In the human brain, GM and CSF are considered to be isotropic, where water molecules diffuse in a random direction [37]. However, in some anisotropic structures of human body, like white matter axonal bundles, the movement of water molecules is restricted [38]. As Figure 3 shows, diffusion parallel to the fiber is faster than in the perpendicular direction. The diffusion direction is largely parallel to the trajectory of the axon, creating an anisotropic process [39]. Therefore, it is assumed that white matter has the highest anisotropy and that diffusion is largest in the tract direction.

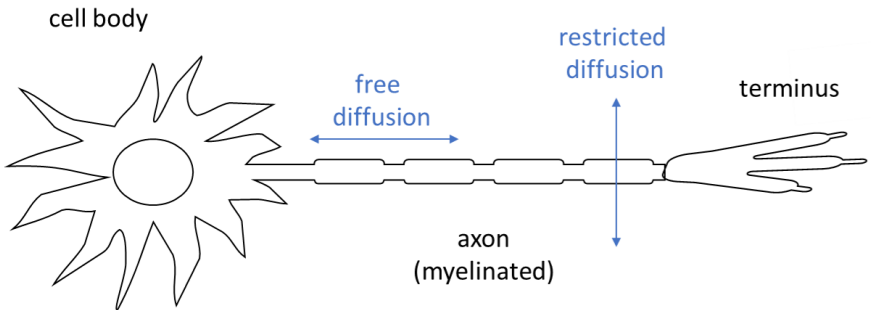

Figure 3. Diffusion in myelinated axon.

Water has different strengths and patterns of diffusion in different tissue structures, and a change in the diffusion pattern might reflect a symptom of disease. For example, when an acute stroke occurs, a disturbance may happen in the diffusion pattern, of an affected area [40]. By examining the changes in diffusion patterns, we can detect the anomaly.

Diffusion weighted magnetic resonance imaging (DWI) is an imaging technique that measures diffusion [41]. It is used to study the diffusion pattern of water molecules and to show the microstructure of tissues. Over approximately 50 msec, water molecules have an average displacement of about 10 μm. They move in a random way of bouncing, crossing, and interacting with various tissue components [40]. DWI measures a property of the displacement distribution of water molecules. The microstructure and geometric organization of tissues, as a result, are observed through DWI.

In DWI, the output signal is determined by the applied diffusion gradients [42]. The gradients are added to a conventional spin-echo MR pulse

sequence, forming a so-called pulsed-gradient spin-echo pulse sequence. Figure 4 shows how the diffusion gradients are applied in the pulse sequence. Two diffusion gradients with the same magnitude G are added to the spin-echo pulse sequence. The first gradient causes spin dephasing while the second gradient causes spin rephasing and they are symmetrically placed around the 180° RF pulse.

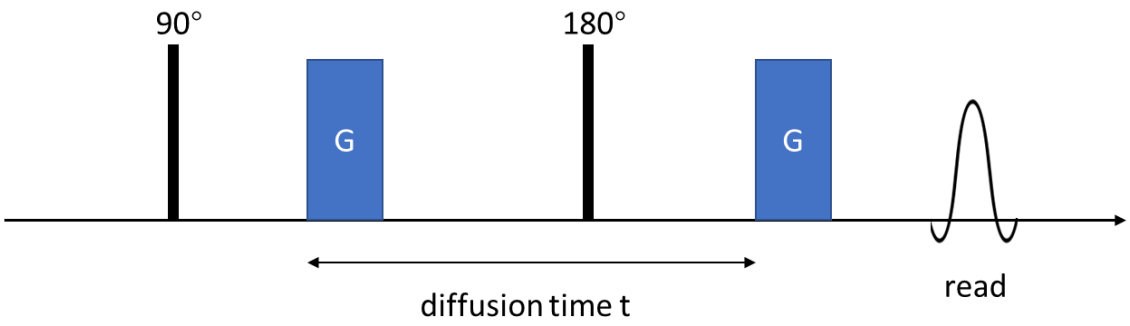

Figure 4. Pulsed-gradient spin-echo sequences.

After the strong magnetic field gradients along certain directions are applied, particle diffusion along those directions during the diffusion time can be measured [42]. Since WM is anisotropic, the signal intensities vary by gradient direction. Applying different gradient along different directions yields different signal intensities in WM.

The diffusion contrast is also affected by the gradient direction. A shell is a set of acquired image volumes with the same b-value but different gradient directions. Generally, at least one b = 0 volume together with shells at higher b-value are acquired in a typical diffusion weighted magnetic resonance

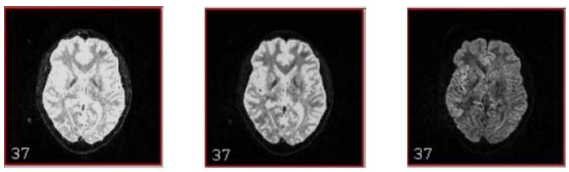

Figure 5. Different DWI images of the same subject with different b-values. (a) diffusion weighted image with b=0. (b) diffusion weighted image with b=1000. (c) diffusion weighted image with b=2000.

imaging (dMRI) protocol.

With different b-values, we can get different DWI images. Figure 5 shows three diffusion weighted images with b-values 0, 250, and 1000. The diffusion weighted image with a b=0 is the brightest since the signal intensity is not attenuated by diffusion. At higher b-values, the diffusion weighted image is more affected by diffusion and the attenuation is more pronounced, as in the darker image in Figure 5(c). Moreover, tissues with high diffusion have lower intensities while tissues with low diffusion are brighter in the diffusion weighted images.

In some diseases, the image intensities in conventional MR sequences like T1 and T2 weighted images do not change much, whereas DWI might show changes. For example, T2 images do not have significant intensity changes in ischemic stroke patients within 8 hours after the onset of stroke. However, evidence of changes can be detected in DWI within 30 minutes after the onset of stroke [43]. DWI is also used to investigate white matter abnormalities in

schizophrenia [44] that do not show on T1 or T2 weighted images. Also, while structural MRI can typically only detect gray matter abnormalities, DWI has proven to be useful in investigating and detecting white matter abnormalities. Therefore, DWI is a good tool for detecting pathological changes like those in early stages of disease or trauma, and it is advantageous to add DWI to conventional MR sequences.

2.4 Diffusion Tensor Imaging

Diffusion tensor imaging (DTI) is a type of DWI. It was first described by Basser et al. [45]. DTI exploits the direction information of water diffusion and it is widely used in extracting the diffusion anisotropy effects and therefore reflecting details of tissue microstructure.

In the diffusion tensor model, it is assumed that the diffusion within tissues are subject to a Gaussian distribution with an anisotropic behavior [46]. For each voxel, the signal measured after applying gradients can be expressed by the equation:

$$S_j = S_0 \exp\left(-b_j \boldsymbol{g}_j^T \boldsymbol{D} \boldsymbol{g}_j\right). \quad (1)$$

In the above equation, S_j corresponds to the signal after applying a gradient

along the $\boldsymbol{g}_j$ direction and with a b-value of b_j. S_0 is the signal before applying any diffusion gradient (with b = 0). $\boldsymbol{D}$ is the 3×3 diffusion tensor and $\boldsymbol{g}_j$ is a unit vector representing the gradient direction.

In equation (1), the diffusion coefficient is a 3×3 diffusion tensor **D** describing anisotropic diffusion.

$$\boldsymbol{D} = \begin{bmatrix} Dxx & Dxy & Dxz \\ Dxy & Dyy & Dyz \\ Dxz & Dyz & Dzz \end{bmatrix}. \quad (2)$$

The diffusion tensor D can have different values in different noncollinear gradient directions. It is a symmetric matric with six unknowns. For determination of the diffusion matrix, at least six diffusion weighted images are needed. However, in practice the more gradient directions, the more robust the results are. The diagonal elements are proportional to apparent diffusion coefficients (ADCs) along the three coordinate directions. The off-diagonal elements of D are proportional to the covariance of these directions. The diffusion tensor fully describes molecular mobility along each direction and correlation between these directions respectively when it satisfies a Gaussian distribution [42].

In Figure 6, the diffusivity along x, y, and z axes are shown in Dxx, Dyy, and Dzz images, respectively.

Figure 6. (a) Dxx image, (b) Dyy image, (c) Dzz image.

If the reference frame [x', y', z'] is along the diffusion frame of the tissue, the off-diagonal terms will no longer exist, and only the diagonal terms are left. In this case, the attenuation is isotropic and is given by

$$A = exp\left(-b_{x'x'}D_{x'x'} - b_{y'y'}D_{y'y'} - b_{z'z'}D_{z'z'}\right), \tag{3}$$

where b_{ii} are the coefficients that replace the scalar b-value in isotropic DWI.

To get ADCs along a local coordinate system per voxel according to the anatomy, the tensor should be diagonalized as follows:

$$\boldsymbol{D} = [\boldsymbol{v}_1 \quad \boldsymbol{v}_2 \quad \boldsymbol{v}_3]^T \begin{bmatrix} \lambda_1 & 0 & 0 \\ 0 & \lambda_2 & 0 \\ 0 & 0 & \lambda_3 \end{bmatrix} [\boldsymbol{v}_1 \quad \boldsymbol{v}_2 \quad \boldsymbol{v}_3]. \tag{4}$$

$\boldsymbol{v}_1$, $\boldsymbol{v}_2$ and $\boldsymbol{v}_3$ are eigenvectors with $\boldsymbol{v}_1$ being the primary direction that has maximum diffusivity. With $\lambda_1 \geq \lambda_2 \geq \lambda_3$, λ_1, λ_2, and λ_3 correspond to the eigenvalues or principal diffusivities, i.e., ADCs along $\boldsymbol{v}_1$, $\boldsymbol{v}_2$, and $\boldsymbol{v}_3$. Therefore, in anisotropic tissues like WM, the diffusion tensor can be considered as an ellipsoid, with eigenvectors being the three directions of

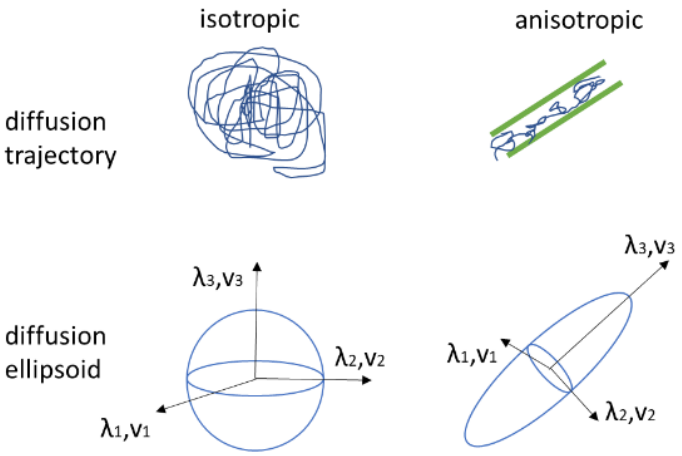

Figure 7. Isotropic and anisotropic diffusion trajectory and ellipsoid model.

coordinates and eigenvalues being the length along each direction. In isotropic tissues like GM and CSF the diffusion tensor can be considered as a ball [47].

2.5 DTI Parameters

DTI parameters provide information on tissue microstructure and architecture [48]. They can then be derived based on the diffusion tensor. The eigenvalues mentioned above are typical DTI metrics. λ_1, which has the largest value among all the three eigenvalues, is called longitudinal or axial diffusivity (AD) [48]; it represents the longitudinal ADC:

$$AD = \lambda_1. \tag{5}$$

The average of λ_2 and λ_3 is called transverse or radial diffusivity (RD) [48]; it

represents the transverse ADC:

$$RD = \frac{\lambda_2 + \lambda_3}{2}. \tag{6}$$

The average of all the three eigenvalues is called mean diffusivity (MD) [48]; it characterizes the overall mean-squared displacement of molecules and the overall restrictions of diffusion:

$$MD = \frac{\lambda_1 + \lambda_2 + \lambda_3}{3}. \tag{7}$$

AD and RD are good metrics to reflect axonal and myelin integrity, respectively, and therefore have good pathologic specificity [10].

Other commonly used invariant indices are the relative anisotropy (RA), fractional anisotropy (FA), and volume ratio (VR). They are all combinations of eigenvalues and are calculated by

$$RA = \frac{\sqrt{\sum_{i=1}^{3}(\lambda_i - \bar{\lambda})^2}}{\sqrt{3\bar{\lambda}}}, \tag{8a}$$

$$FA = \sqrt{\frac{3\sum_{i=1}^{3}(\lambda_i - \bar{\lambda})^2}{2\sum_{i=1}^{3}\lambda_i^2}}, \tag{8b}$$

and

$$VR = \frac{\lambda_1\lambda_2\lambda_3}{\bar{\lambda}^3}. \tag{8c}$$

RA is the ratio of the anisotropic part of **D** to the isotropic part; it is a normalized standard deviation [49]. The range of RA is from 0 to $\sqrt{2}$, with lower values indicating more isotropic characteristics and higher values indicating more anisotropic characteristics [49]. FA is a fraction also showing how much **D** can be described as anisotropic [49]. The value varies from 0 to 1, with values close to 1 representing highly anisotropic diffusion [47]. In the region of white matter tracts, the value of FA varies between 0.4 and 0.8 while in the region of gray matter, the value of FA is below 0.2 [50]. In CSF, the value of FA is close to 0 [50].

As mentioned before, anisotropic diffusion tensors can be represented by an ellipsoid while isotropic diffusion tensors can be represented by a ball [47]. VR shows the ratio of the volume of the ellipsoid to a sphere volume with radius equal to principal eigenvalue λ_1 [51]. The range is 0 to 1, with values close to one indicating isotropic diffusion (which is the opposite of RA and FA) [51]. Many studies prefer to use $(1 - VR)$ instead of VR [51], to make the scale similar to RA and FA.

FA is a good indicator of the strength of directional diffusion, and it is also thought to mark the integrity of WM [52]. The principal fiber orientation can be estimated by the direction of the highest diffusivity in anisotropic areas [48]. However, in voxels with crossing fibers, FA is lower, and the tensor ellipsoid is oblate (with two crossing fibers), i.e., shape like a pancake, or

spherical (with three crossing fibers) [47]. In that case, the differences of FA are hard to interpret.

A decrease of FA and increase of MD could be related to tissue breakdown or loss of structure [48]. A decrease of AD and increase of RD could be associated with axonal and myelin breakdown, respectively [48].

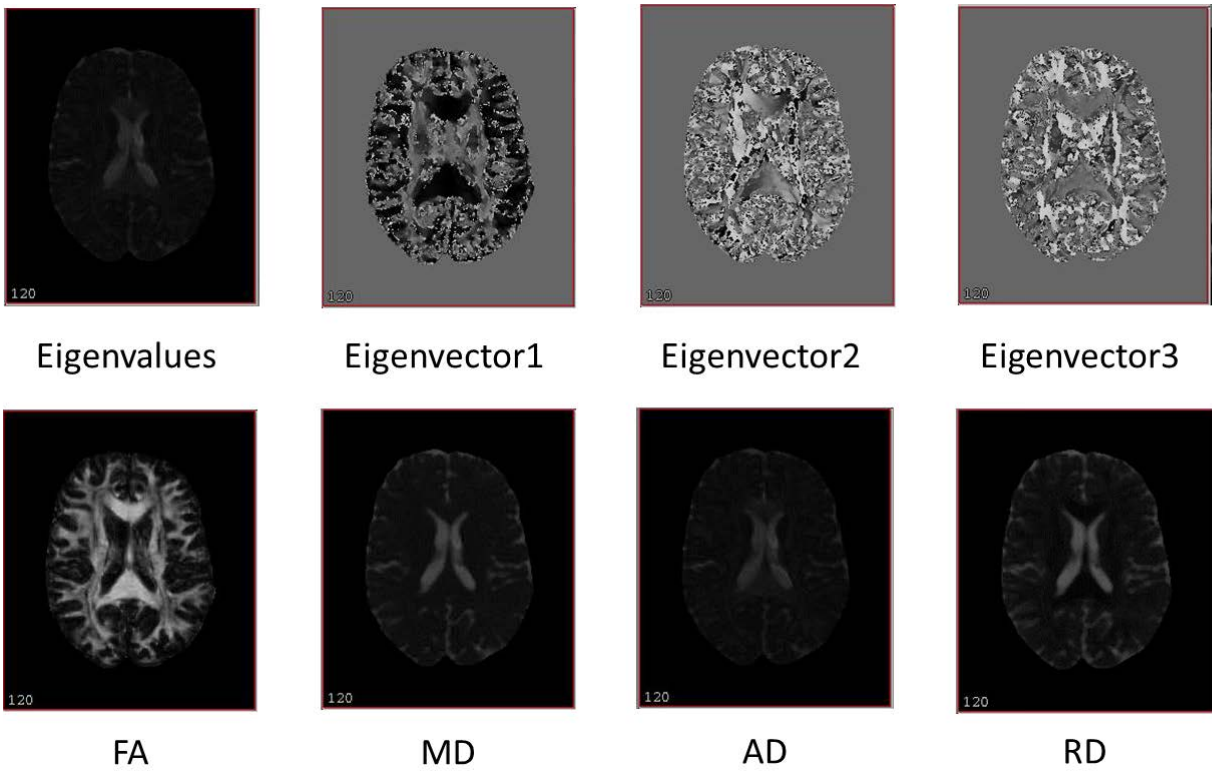

Figure 8. DTI parameters.

Different acquisition parameters cause different DTI metric values. For example, FA is affected by the number of gradient directions and spatial resolution while MD is influenced by diffusion sensitization [53]. According to published studies, FA and MD are more reproducible and repeatable with

more gradient directions [54]. It is considered that robust results can be obtained using 30 gradient directions with a b-value of 1000 s/mm^2.

2.6 Diffusion Kurtosis Imaging

Diffusion kurtosis imaging (DKI) is an advanced neuroimaging modality which is an extension of diffusion tensor imaging. DKI measures the kurtosis (skewed distribution) of water diffusion based on a probability distribution function.

DTI makes sense when the diffusion of water molecules follows a Gaussian distribution. DKI, on the other hand, does not make the Gaussian assumption [55]. It uses stronger gradients (higher b-values) and longer echo times. DKI protocols differ from DTI protocols in requiring at least 3 b-values (as compared to 2 b-values for DTI) and at least 30 independent diffusion gradient directions (as compared to 6 for DTI). In typical DTI, the images are acquired at b=0 and b=1000 s/mm^2. However, in DKI, typical protocols for brain have b-values of 0, 1000, 2000 s/mm^2 with multiple diffusion directions [56].

DKI provides a high order diffusion measurement of water distribution and also quantifies diffusion restriction caused by, for example, axonal walls.

Kurtosis, denoted by the dimensionless parameter K, is a long recognized statistical metric for quantifying the shape of a probability distribution [57]. Diffusion in pure fluids is Gaussian, but biological tissues are characterized by a positive diffusion kurtosis. This reflects the heterogeneous diffusion environments experienced by water molecules as they encounter barriers, move between compartments, and undergo chemical exchange [56]. A water molecule diffusing according to a K>0 distribution would typically not travel as far in a given time interval as one that followed Gaussian (K=0) statistics [56]. Typical calculated kurtosis values might range from K=0 for CSF to K=0.7 for GM to K=1.0 for WM.

Analogous to DTI it is possible to create diffusion kurtosis tensors and, for example, estimate axial and radial components of kurtosis. At least 15 different diffusion directions and two non-zero b-values must be probed to create a tensor. Calculation of diffusion metrics from DKI are similar to those calculated from DTI. The typical kurtosis metrics are mean, axial, and radial kurtosis [58]. DTI-derived diffusion parameters (RD, FA and MD) have been shown to be sensitive to detect abnormality in white matter regions with coherent fiber arrangement; however, the kurtosis parameters (MK and AK) have been shown to be sensitive to reveal abnormality in white matter regions with complex fiber arrangement [59].

2.7 Summary

In this chapter we have reviewed the main modalities that related to the study.

With good contrast between CSF and other tissues as well as moderate contrast between WM and GM, MP-RAGE images have been widely used for classifying brain tissues in voxel-based, detecting pathological changes of the brain, and estimating regional brain volume abnormalities associated with brain functions.

In the human brain, GM and CSF are considered to be isotropic and therefore the DW signal intensities of GM and CSF are determined only by ADC and are invariant to the gradient directions. On the contrary, WM is anisotropic and the signal intensities vary by gradient direction. Applying different gradient along different directions yields different signal intensities in white matter. Therefore, DWI is useful in investigating and detecting white matter abnormalities. Particularly, DTI is widely used in extracting the diffusion anisotropy effects and reflecting details of tissue microstructure.

DTI parameters provide information on tissue microstructure and architecture. FA is a good indicator of the strength of directional diffusion, and it is also thought to mark the integrity of WM. MD characterizes the overall mean-squared displacement of molecules and the overall restrictions

of diffusion. AD and RD are good metrics to reflect axonal and myelin integrity, respectively, and therefore have good pathologic specificity.

DKI extends conventional DTI by estimating the kurtosis of the water diffusion probability distribution function. In contrast to DTI, DKI does not make the Gaussian assumption on diffusion. DKI protocols differ from DTI protocols in using stronger gradients (higher b-values) and longer echo times and requiring at least 3 b-values and at least 30 independent diffusion gradients. Analogous to DTI, it is possible to create diffusion kurtosis tensors and estimate axial and radial components of kurtosis. The typical kurtosis metrics are mean, axial, and radial kurtosis.

Chapter 3 Data and Image Acquisition

3.1 Data

Imaging data were acquired by collaborators at the University of Maryland (UMD). The data include 76 mTBI subjects from four different visits and 51 healthy subjects with at most two visits. The first visit of the mTBI subjects was within ten days of injury, the second visit was after one month, the third visit was after six months, and the last visit was after 18 months. Among all 76 mTBI patients, 56 are male and 20 are female. Of the 51 healthy controls, 30 are male and 21 are female; they all had two visits within an interval of six months. The chi-square value shows no significant difference in the proportion of gender. The average age of mTBI patients is 43.30 with a standard deviation of 14.56 while the average age of healthy controls is 40.43 with a standard deviation of 16.05. The p value of ages between mTBI

patients and healthy controls is 0.19, showing no significant difference in age between the mTBI group and the healthy control group. Controls had slightly more education (mean=15.47 years) than TBI patients (mean=13.88 years) (p=0.0004).

The Glasgow Coma Score (GCS) is a scoring system used to estimate coma severity according to criteria from different fields including vision, verbal, and motor. It is commonly used to estimate TBI severity. The range of GCS in our patient cohort is from 13 to 15. The lower the value, the more severe the disease is, and the patients are more likely to be in a coma state. The average GCS in our patient cohort is 14.76 with a standard deviation of 0.39, which means that most patients have mild TBI.

Table 2. Demographics.

	TBI	Control	p
Age, years (SD)	43.30(14.56)	40.43(16.05)	0.19
Education, years (SD)	13.88(2.18)	15.47(1.87)	0.0004
Male, n (%)	56(0.74)	30(0.59)	0.08
Female, n (%)	20(0.26)	21(0.41)	0.08
GCS	14.76(0.39)	N/A	N/A

3.2 Image Acquisition

All MR images were obtained on Siemens Tim Trio 3T MRI scanners using 12 channel receiver head coils. High-resolution three-dimensional T1-weighted images were acquired using the magnetization prepared rapid acquisition of gradient echoes (MP-RAGE) pulse sequence with two variations: (1) TE = 3.44 ms, TR = 2250 ms, TI = 900 ms, flip angle = 9°, FOV = 230 mm, resolution = 0.9 x 0.9 x 2 mm^3, and 72 axial slices parallel to anterior and posterior commissure points (AC-PC)); (2) TE = 2.91 ms, TR = 2300 ms, TI = 900 ms, flip angle = 9°, FOV = 256mm, resolution = 1×1×1 mm^3, and 196 sagittal slices to cover the whole head. Other conventional MRI performed included T2 weighted (TE = 83 ms, TR = 5690 ms, FOV = 230 mm, resolution = 0.6 x 0.4 x 5 mm^3, and 26 axial slices with 20% gap), FLAIR (TE = 77 ms, TR = 8000 ms, TI = 2500 ms, FOV = 230 mm, resolution = 1.2 x 0.9 x 5 mm^3, and 26 axial slices with 20% gap), and susceptibility weighted imaging (TE = 20ms, TR = 28ms, flip angle = 15°, FOV = 230 mm, resolution = 0.8 x 0.7 x 2 mm^3, and 72 axial slices).

For the DWI acquisition, diffusion-weighted images were acquired with a twice refocused, single shot, spin-echo EPI sequence. Thirty diffusion directions with two b-values (1000 and 2000 sec/mm^2), along with four b0 images and two repetitions were acquired. Parallel imaging was used with an

acceleration factor of two at a TE = 101 msec and TR = 6000 msec. The in-plane resolution was 2.7 mm^2, with a 7/8 partial Fourier factor, at a slice thickness of 2.7 mm to cover the whole brain. The total image acquisition time was about 13 min.

Chapter 4 Volume Comparison

4.1 Brain Segmentation

Both MP-RAGE and T2 images were used to yield brain segmentations and labeling. The images were first preprocessed by N4 bias correction [60] and registered to MNI space. Brain masks were generated using MONSTR [61] (Multi-cONtrast brain STRipping) and then whole brain segmentation was done by MaCRUISE [62]. MaCRUISE is a method for whole brain segmentation and cortical surface reconstruction. It segments the brain into 133 labels based on multi-atlas segmentation applied to T1 weighted images. See Figure 9 for a block diagram of MaCRUISE.

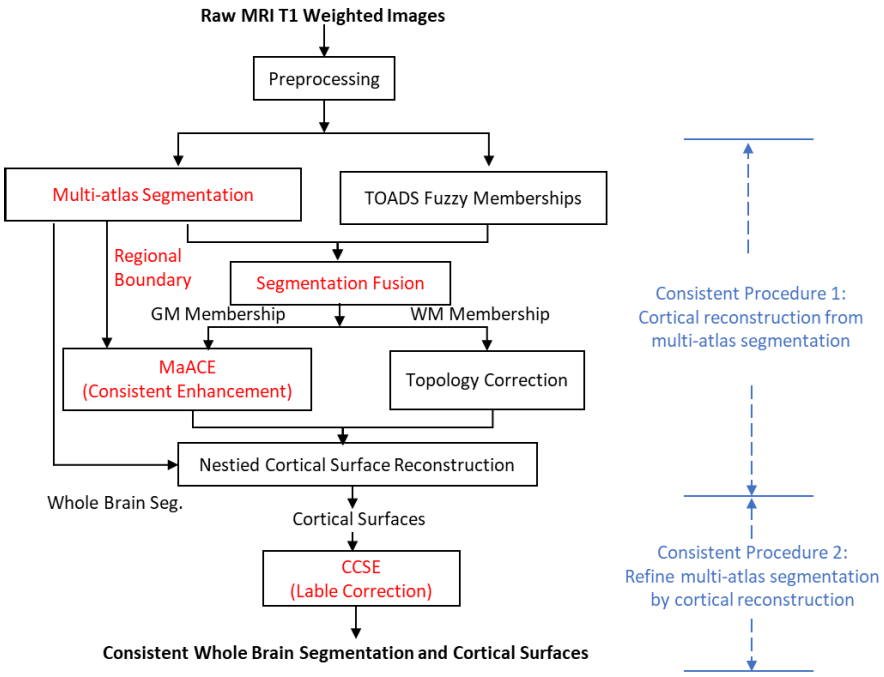

Figure 9. Block diagram of MaCRUISE 62.

An example of an MaCRUISE segmentation result is shown in Figure 10.

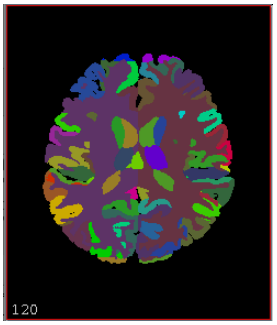

Figure 10. An example result of MaCRUISE segmentation.

After segmenting the brain into 133 labels using MaCRUISE [62], the volume of each label was calculated. The volume was calculated by computing the number of voxels in each label and multiplying this number by

the volume of a voxel. The volumes of ventricular CSF, cerebral white matter, cerebral gray matter, and the whole brain parenchyma (VBP) were calculated by combining the volumes of their constituent labels. Ventricular CSF is the combination of the 3rd ventricle, 4th ventricle, left caudate, right caudate, left lateral ventricle, and right lateral ventricle. Cerebral white matter includes the left cerebral white matter and the right cerebral white matter. The original labels and adding these combined labels yield a total of 137 labels that were studied.

4.2 Hypothesis

It was hypothesized that mild TBI patients would show a decrease in WM as well as GM volumes while an increase in CSF volume compared with healthy controls. It was hypothesized that mild TBI patients would show a decrease in white matter volume and gray matter volume while showing increase in ventricular CSF over time. A cross-sectional comparison of patients and healthy controls and a longitudinal comparison were conducted in this study to verify the hypotheses.

4.3 Cross-sectional Comparison

A cross-sectional study compares the differences among selected subjects, e.g., patients and healthy controls. Subject images are assumed to be collected at a single point in time, rather than at multiple time points. It was hypothesized that mild TBI patients would show a decrease in WM as well as GM volumes while an increase in CSF volume compared with healthy controls. We carried out cross-sectional comparisons of the volumes of different ROIs using two-way Analysis of Covariance (ANCOVA) in R [63]. Since healthy controls only have two visits with an interval of six months, we chose to use only two of the visits of mild TBI patients for cross-sectional analysis: Visit 1 (within ten days post-injury) and Visit 3 (six months post-injury).

The main fixed effects for this model are visit, group (mTBI, control), and their interactions. Age, sex, ICV, sequence type (axial, sagittal) are covariates which have potential effects on the dependent variables. The intracranial volume was computed using the results of MONSTR [61], a multi-contrast brain isolation method that uses both T1 and T2 weighted images, which gives us more accurate results of than other methods, which use only T1-weighted images. In our data, T1 images were acquired with two types of pulse sequences–axial and sagittal. Since the two types may have different

impacts on brain volume computation, the sequence type was also incorporated as a covariate.

In this part, data from 42 healthy controls and 65 patients in Visit 1 (within ten-days injury) and 32 healthy controls and 51 patients in Visit 2 (six months post-injury) were examined. As seen in the CONSORT (Consolidated Standards of Reporting Trials) figure showing the flow of subjects through the trial.

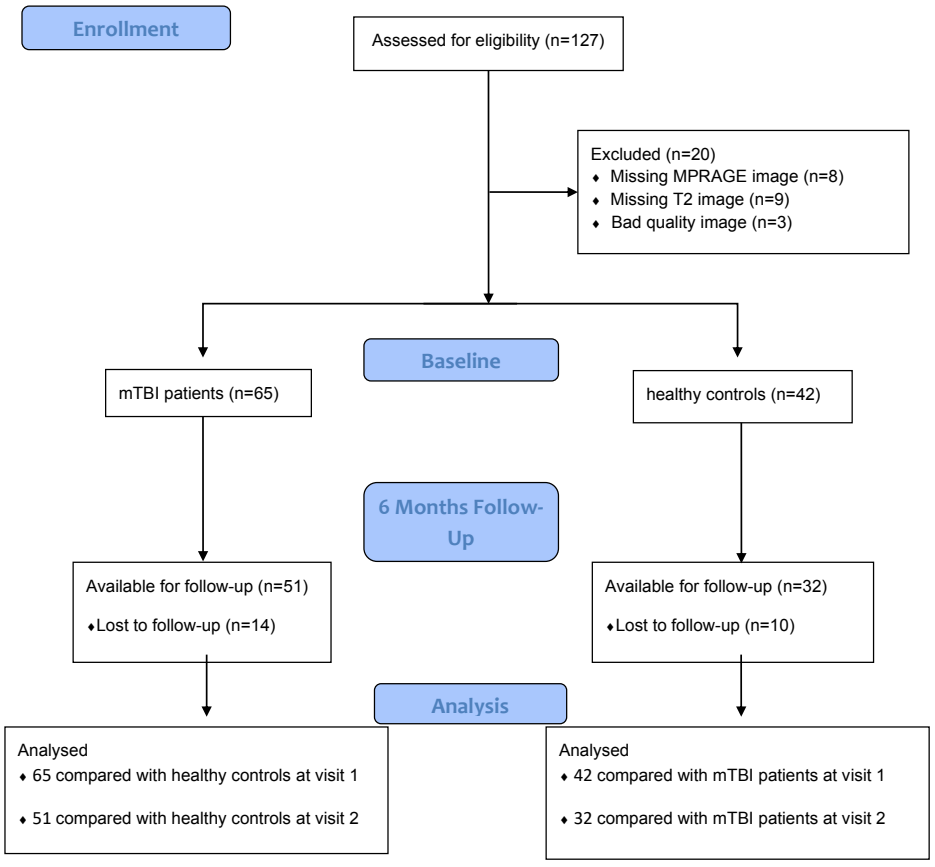

Figure 11. CONSORT figure in cross-sectional volumetric study.

Of all the 137 regions of interests, six were found to have the significant

difference between mTBI group and HC group from the results of two-way ANCOVA. They are the right fusiform gyrus, right postcentral gyrus medial segment, left postcentral gyrus medial segment, left posterior insula, left superior frontal gyrus, and right transverse temporal gyrus.

The means for groups that are adjusted for the means of other factors in the model are called least square means. Least square means and their standard errors are calculated and shown in Table 3. The confidence intervals were adjusted for multiple comparisons.

Table 3. Group information after adjusted for means of other factors in the model.

ROIs	Visit	group	lsmean/mm^3	SE/ mm^3	df	lower CL/mm^3	upper CL/mm^3
Right fusiform gyrus	1	HC	8089	134	182	7751	8427
	2	HC	8207	144	182	7843	8570
	1	patient	7883	113	182	7598	8168
	2	patient	7726	115	182	7436	8015
Right postcentral gyrus medial segment	1	HC	1022	30.3	182	946	1098
	2	HC	1056	32.5	182	974	1138
	1	patient	917	25.5	182	853	981
	2	patient	893	25.9	182	827	958
Left postcentral gyrus medial segment	1	HC	1068	31.1	182	990	1147
	2	HC	1054	33.4	182	970	1138
	1	patient	985	26.2	182	919	1051
	2	patient	945	26.7	182	878	1012
Left posterior insula	1	HC	2571	43.9	182	2461	2682
	2	HC	2472	47.2	182	2354	2591
	1	patient	2599	37	182	2506	2692
	2	patient	2634	37.6	182	2540	2729
Left superior frontal gyrus	1	HC	17083	283	182	16371	17794
	2	HC	16936	304	182	16171	17701
	1	patient	16203	239	182	15603	16803
	2	patient	16333	242	182	15723	16943
Right transverse temporal gyrus	1	HC	1542	49.8	182	1417	1668
	2	HC	1465	53.6	182	1330	1599

Right transverse temporal gyrus	1	patient	1649	42	182	1543	1755
	2	patient	1650	42.7	182	1543	1758

Note. lsmean refers to least squared means, SE refers to standard error, df refers to degree of freedom, and CL refers to confidence limit.

Table 4 shows the pairwise difference and significance between different groups in different visits. Tukey p-value corrections were done to prevent small p-values (below 5%) from happening by chance. "1, HC" means healthy controls at Visit 1 while "2, patient" means mTBI patients at Visit 2. "1, HC-2, HC" and "1, patient-2, patient" represent within group difference over time. "1, HC-1, patient" and "2, HC-2, patient" represent between group difference at the same visit.

Table 4. Pairwise comparison of groups.

ROIs	comparison	estimated difference/mm^3	SE/mm^3	df	t ratio	corrected p-value
Right fusiform gyrus	1,HC-2,HC	-118	181	182	-0.651	0.9152
	1,HC-1,patient	206	157	182	1.314	0.5553
	2,HC-2,patient	481	177	182	2.725	0.0353*
	1,patient-2,patient	158	146	182	1.082	0.701
Right postcentral gyrus medial segment	1,HC-2,HC	-33.8	40.7	182	-0.831	0.8398
	1,HC-1,patient	105.2	35.3	182	2.978	0.0172*
	2,HC-2,patient	163.3	39.8	182	4.104	0.0004***
	1,patient-2,patient	24.3	32.8	182	0.74	0.881
Left postcentral gyrus medial segment	1,HC-2,HC	14	41.8	182	0.334	0.9871
	1,HC-1,patient	82.9	36.3	182	2.283	0.1059
	2,HC-2,patient	109.6	40.9	182	2.681	0.0397*
	1,patient-2,patient	40.7	33.7	182	1.208	0.6224
Left posterior insula	1,HC-2,HC	98.8	59	182	1.673	0.3411
	1,HC-1,patient	-27.6	51.3	182	-0.538	0.9496
	2,HC-2,patient	-161.8	57.7	182	-2.803	0.0285*
	1,patient-2,patient	-35.4	47.6	182	-0.744	0.879
Left superior frontal gyrus	1,HC-2,HC	147	380	182	0.386	0.9804
	1,HC-1,patient	880	330	182	2.663	0.0416*
	2,HC-2,patient	603	372	182	1.62	0.3697

Left superior frontal gyrus	1,patient-2,patient	-130	307	182	-0.424	0.9742
	1,HC-2,HC	77.657	67	182	1.159	0.6537
Right transverse temporal gyrus	1,HC-1,patient	-106.855	58.2	182	-1.836	0.2597
	2,HC-2,patient	-185.492	65.5	182	-2.831	0.0263*
	1,patient-2,patient	-0.979	54	182	-0.018	1

Note. "1,HC" means healthy controls at Visit 1 while "2,patient" means mTBI patients at Visit 2. SE represents standard error and df represents degree of freedom.

$*$ indicates P $\leqslant$ 0.05. $**$ indicates P $\leqslant$ 0.01. $***$ indicates P $\leqslant$ 0.001.

Figure 12 shows the corresponding pairwise comparison plots with error bars representing the standard error of means in units of y-axis is mm^3. The blue lines refer to the results from healthy controls and the yellow lines refer to the results from the mTBI patients. The significance is shown on top of the error bars.

For between group comparison, in general, the volumes of the right fusiform gyrus, right postcentral gyrus medial segment, left postcentral gyrus medial segment, left superior frontal gyrus show significantly lower values in mTBI patients than healthy controls. The volumes of left posterior insula and right transverse temporal gyrus show significantly higher values in mTBI patients than healthy controls. There are significant differences between patients and healthy controls on Visit 2 for the left postcentral gyrus medial segment (corrected p=0.0397), right postcentral gyrus medial segment (corrected p=0.0004), right fusiform gyrus (corrected p=0.0353), left posterior insula (corrected p=0.0285), and right transverse temporal gyrus (corrected p=0.0263). However, in left superior frontal gyrus area, the significance

(corrected p=0.0416) is shown on Visit 1. In the right postcentral gyrus medial segment area, there are significance on both Visit 1 (corrected p=0.0172) and Visit 2 (corrected p=0.0004).

For within group comparison, there shows no significant difference in either the mTBI group or healthy controls over six months.

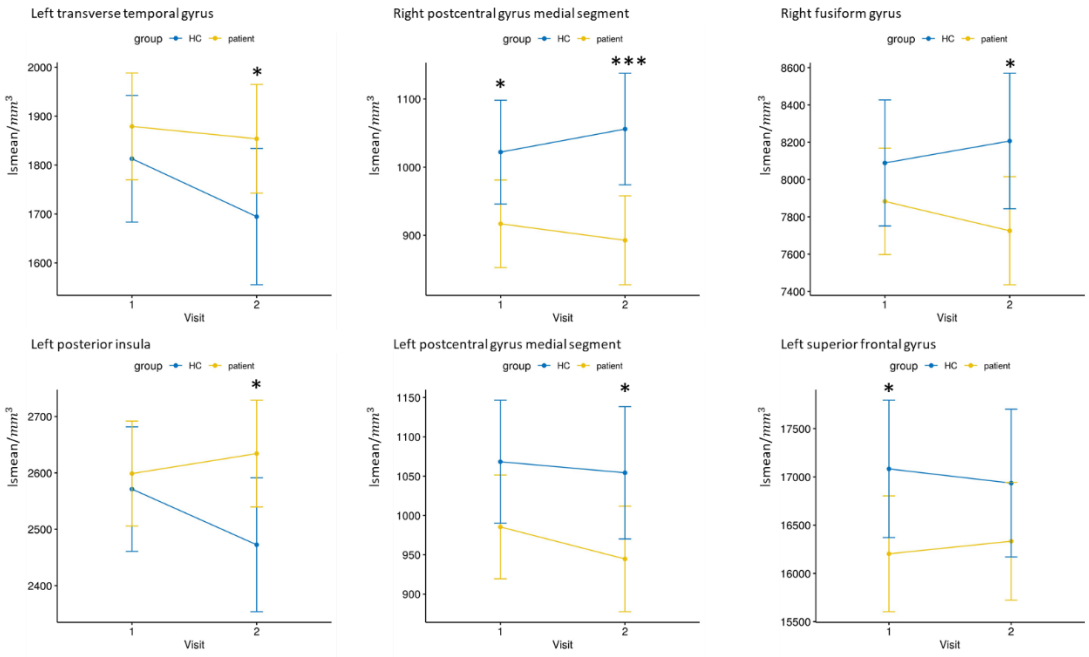

Figure 12. Pairwise comparison plots of right transverse temporal gyrus, right postcentral gyrus medial segment, right fusiform gyrus, left posterior insula, left postcentral gyrus medial segment, left superior frontal gyrus, and with error bars. The error bars represent the confidence intervals of the means.

4.4 Longitudinal Comparison

Longitudinal studies were done by measuring repeatedly over certain periods of time on a sample of subjects [64]. This differs from cross-sectional

studies, which measure a sample of subjects at only one time point. Through longitudinal studies, developments or changes in certain characteristics or performance of the target subjects can be observed not only at a group level but also at an individual level.

For longitudinal studies that repeat the measurement of subjects over time, the linear mixed effects model is commonly used for data analysis [65]. An assumption of the model is that all the individuals have their own response trajectories over time. In this model, there are "fixed" effects, which are the mean responses of variables to be shared by all individuals. "Random" effects also exist in this model; these are subject-specific and are unique to certain individuals. The model gets its name "mixed" since it involves both fixed and random effects. In longitudinal studies, fixed effects generally incorporate the effects due to treatment, exposure, and background characteristics of the subjects while random effects are more flexible in the way of modeling correlation and variability of the repeated measurements [66].

Longitudinal comparison of mTBI patients over four visits were examined. Since some visits were missing for some of the subjects, not all visits have the same number. In this part, there are 65 data sets for Visit 1, 57 data sets for Visit 2, 55 data sets for Visit 3, and 48 data sets for Visit 4.

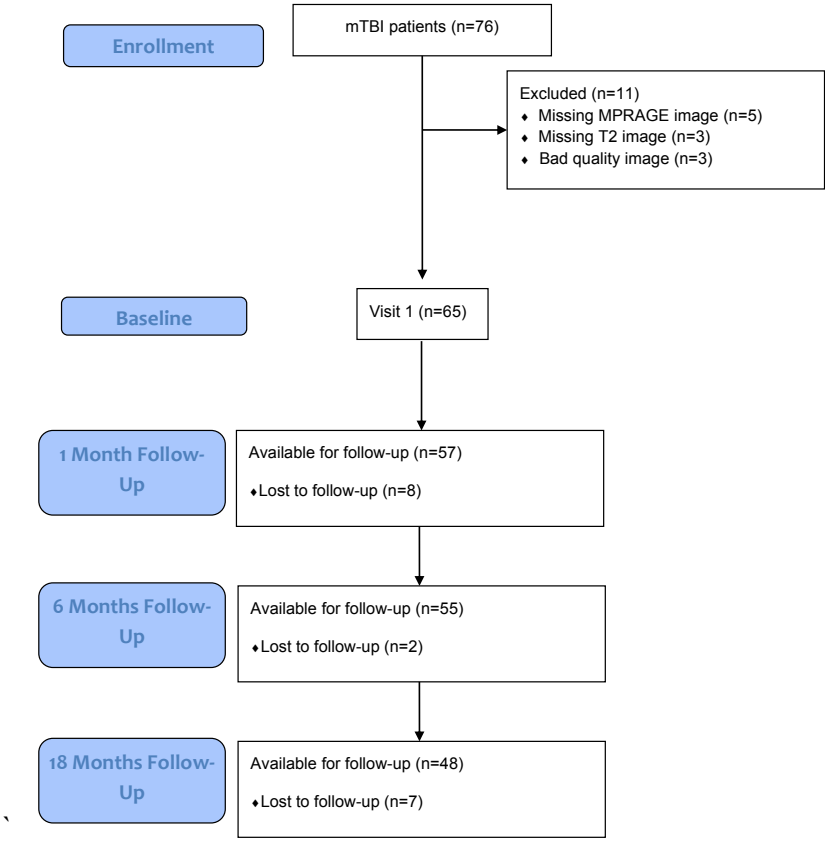

Figure 13. CONSORT figure in longitudinal volumetric study.

Statistical tests were performed on structural volumes using the linear mixed effects model in R [63]. The linear mixed model has the advantage of dealing with missing data. Assuming the missing data is "missing at random", it uses maximum likelihood to get estimates of the parameters of the model and give unbiased results in the presence of missing data.

It is hypothesized that mild TBI patients would show a decrease in white matter volume and gray matter volume while showing increase in ventricular CSF over time. This hypothesis was tested using a linear mixed effects model.

In this study, there are many factors such as sex, age, intracranial volume (ICV), and sequence type that could affect the volumes of the regions of interests. Linear mixed effects regression model was used to study the relationship of those factors with baseline and longitudinal change in each region individually. The fixed effects are visit, ICV, sequence type (axial and sagittal), sex, age, interaction between ages and visits, and interaction between sex and visits. The effects of visit are the main effect we are trying to examine while sex, age, ICV, and sequence type are the covariates since there are known or potential effects on brain structure. The random effect is the individual effect. Type I error levels were being used to test whether the fixed effects are significantly different.

Since the analysis is a multiple comparison, p-value corrections should be made for controlling the type I error. The Tukey method was used here as a less stringent method to prevent small p-values (below 5%) from happening by chance.

The results reveal that after Tukey p-value corrections, of all the regions of interest, the left accumbens area, right amygdala, left frontal operculum, left frontal operculum, right occipital fusiform gyrus, left planum temporale, right temporal pole, left lateral ventricle, 3rd ventricle, and ventricular CSF show significant difference among visits.

The means for groups that are adjusted for means of other factors in the

model are called least square means. Least square means and their standard errors are calculated and shown in Table 5. The confidence intervals were adjusted for multiple comparisons.

Table 5. Group information after adjusted for means of other factors in the model.

ROIs	Visit	lsmean/mm^3	SE/ mm^3	df	lower CL/mm^3	upper CL/mm^3
Left accumbens area	1	440	12.7	75.4	408	472
	2	432	12.9	80.7	399	465
	3	424	12.9	81.9	391	457
	4	420	13.4	91.9	386	454
Right amygdala	1	1009	15.2	79.9	971	1048
	2	1012	15.6	87.3	972	1051
	3	989	15.7	89	949	1029
	4	976	16.4	102.5	934	1017
Left frontal operculum	1	1771	48.4	68.6	1647	1894
	2	1753	48.7	70.3	1628	1878
	3	1726	48.8	70.6	1602	1851
	4	1722	49.4	74	1596	1848
Right occipital fusiform gyrus	1	3741	81.3	72.4	3534	3949
	2	3768	82.4	76.2	3558	3979
	3	3692	82.6	77	3481	3903
	4	3641	84.8	84.3	3425	3857
Left planum temporale	1	2486	84.4	68.1	2270	2702
	2	2442	84.9	69.5	2224	2659
	3	2434	84.9	69.8	2217	2651
	4	2409	85.9	72.6	2190	2629
Right temporal pole	1	7887	147	71.8	7512	8263
	2	7842	149	75.3	7462	8222
	3	7809	149	76	7428	8190
	4	7686	153	82.7	7296	8075
Left lateral ventricle	1	11173	812	68	9095	13250
	2	11943	816	69.3	9856	14030
	3	11771	817	69.6	9683	13859
	4	12144	825	72.3	10036	14253

ROIs	Visit	lsmean/mm^3	SE/ mm^3	df	lower CL/mm^3	upper CL/mm^3
3rd ventricle	1	914	72.3	70.5	729	1098
	2	983	73	73.3	797	1170
	3	979	73.1	73.8	793	1166
	4	1007	74.6	79.3	817	1198
Ventricular CSF	1	31045	1670	66.8	26770	35319
	2	32229	1674	67.4	27945	36512
	3	31956	1674	67.4	27672	36240
	4	32448	1682	68.7	28145	36752

Note. lsmean refers to least squared means, SE refers to standard error, df refers to degree of freedom, and CL refers to confidence limit.

Table 6 shows the pairwise difference and significance in different visits. The p-value was corrected for multiple comparison.

Table 6. Pairwise comparison of different visits.

ROIs	comparison	estimated difference/mm^3	SE/mm^3	df	t ratio	corrected p-value
Left accumbens area	1-2	7.75	6.48	110	1.197	0.63
	1-3	15.79	6.79	111	2.324	0.0987
	1-4	20.35	7.55	111	2.693	0.0402*
	2-3	8.04	7.21	111	1.114	0.6817
	2-4	12.59	7.95	111	1.585	0.3915
	3-4	4.56	8.01	111	0.569	0.9412
Right amygdala	1-2	-2.35	9.18	111	-0.256	0.9941
	1-3	20.41	9.62	112	2.123	0.1523
	1-4	33.52	10.69	113	3.137	0.0115*
	2-3	22.76	10.21	112	2.229	0.1218
	2-4	35.87	11.24	113	3.191	0.0098*
	3-4	13.11	11.34	112	1.156	0.6555
Left frontal operculum	1-2	17.52	14.2	108	1.231	0.6085
	1-3	44.3	15	109	2.962	0.0193*
	1-4	48.35	16.6	108	2.906	0.0227*
	2-3	26.78	15.9	109	1.687	0.3355
	2-4	30.83	17.5	108	1.763	0.297
	3-4	4.05	17.6	109	0.229	0.9957
Right occipital fusiform gyrus	1-2	-26.9	35.3	109	-0.761	0.8717
	1-3	49.4	37	110	1.333	0.5439
	1-4	100.7	41.2	110	2.444	0.0749

ROIs	comparison	estimated difference/mm^3	SE/mm^3	df	t ratio	corrected p-value
Right occipital fusiform gyrus	2-3	76.2	39.3	110	1.939	0.2181
	2-4	127.6	43.3	110	2.944	0.0204*
	3-4	51.3	43.7	110	1.175	0.6441
Left planum temporale	1-2	44.62	22.7	108	1.969	0.2063
	1-3	52.48	23.8	108	2.202	0.1291
	1-4	76.98	26.5	108	2.904	0.0228*
	2-3	7.86	25.3	108	0.311	0.9895
	2-4	32.37	27.9	108	1.161	0.6524
	3-4	24.51	28.1	109	0.871	0.8196
Right temporal pole	1-2	45.3	61.1	109	0.742	0.8801
	1-3	78.3	64.1	110	1.221	0.6152
	1-4	201.6	71.4	110	2.825	0.0283*
	2-3	33	68.1	110	0.484	0.9625
	2-4	156.3	75	110	2.083	0.1653
	3-4	123.3	75.7	110	1.63	0.3664
Left lateral ventricle	1-2	-770	213	108	-3.622	0.0025*
	1-3	-598	223	108	-2.674	0.0423*
	1-4	-971	249	108	-3.906	0.0009*
	2-3	172	237	108	0.725	0.8869
	2-4	-201	261	108	-0.77	0.8676
	3-4	-373	264	108	-1.416	0.4923
3rd ventricle	1-2	-69.8	26.9	108	-2.591	0.0523
	1-3	-65.7	28.3	109	-2.323	0.0992
	1-4	-93.8	31.5	109	-2.979	0.0185*
	2-3	4.1	30	109	0.136	0.9991
	2-4	-24	33.1	109	-0.724	0.8875
	3-4	-28	33.4	109	-0.84	0.8351
Ventricular CSF	1-2	-1184	291	107	-4.075	0.0005*
	1-3	-911	306	108	-2.979	0.0185*
	1-4	-1403	340	108	-4.126	0.0004*
	2-3	273	325	108	0.84	0.8351
	2-4	-219	358	107	-0.613	0.9277
	3-4	-492	361	108	-1.363	0.5253

Note. "1-2" means comparison between Visit 1 and Visit 2. SE represents standard error and df represents degree of freedom.

$*$ indicates $P \leqslant 0.05$. $**$ indicates $P \leqslant 0.01$. $***$ indicates $P \leqslant 0.001$.

Figures 14 and 15 show pairwise comparison plots with means and error

bars for the left accumbens area, right amygdala, left frontal operculum, left frontal operculum, right occipital fusiform gyrus, left planum temporale, right temporal pole, left lateral ventricle, 3rd ventricle, and ventricular CSF. The significance is shown on top of the error bars and the error bars represent the standard error.

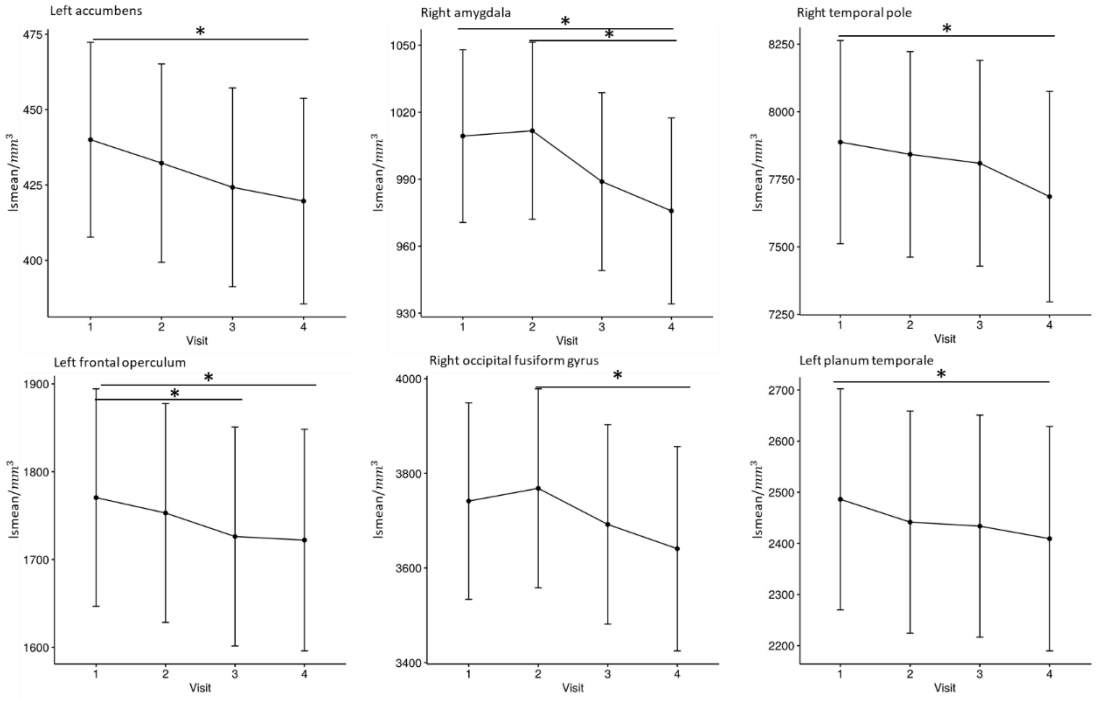

Figure 14. Least squared means of left accumbens area, right amygdala, right temporal pole, left frontal operculum, left frontal operculum, right occipital fusiform gyrus, and left planum temporale with error bars over four visits. The error bars represent the standard error of least squared means.

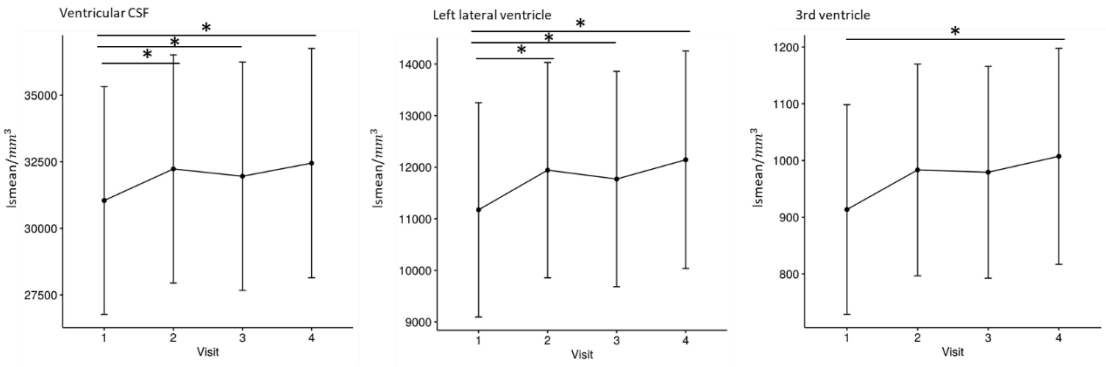

Figure 15. Least squared means of ventricular CSF, left lateral ventricle, and 3rd ventricle over four visits. The error bars represent the standard error of least squared means.

From the results, the left lateral ventricle, 3rd ventricle, and ventricular CSF show increasing trends over the four visits. However, the left accumbens, right amygdala, left ventral diencephalon, left frontal operculum, left frontal operculum, right occipital fusiform gyrus, left planum temporale, and right temporal pole show decreasing trends. Those areas are all gray matter areas. In contrast to what we predicted, no significant regional volume changes were found in the volumes of the label cerebral WM, GM, and VBP. A decreasing trend was only found in some of the smaller gray matter areas.

Chapter 5 DTI Parameter Comparison

5.1 Hypothesis

White matter is a likely candidate for volume loss [64]. Therefore, the investigation of white matter microstructural changes might be present. It was hypothesized that mild TBI patients would show decreased FA, increased MD, decreased AD, and increased RD compared to healthy controls. It was also hypothesized that the mTBI patients would show more decreased FA, increased MD, decreased AD, and increased RD over time. A cross-sectional comparison of patients and healthy controls and a longitudinal comparison were conducted in this study to verify the hypotheses.

5.2 IIT Atlas

DTI parameters in the white matter were examined, using white matter tract segmentation and diffusion tensor metrics. Preprocessing of the diffusion data included registration of each diffusion weighted image to the associated mean b0 and some distortion corrections. Corrections were made for susceptibility-induced distortions as well as corrections for eddy currents and subject movement. Tensor estimation was performed using DTIFIT from FSL [67], which fits a diffusion tensor model at each voxel and computes tensors. The tensors were then registered to the Illinois Institute of Technology (IIT) human brain atlas to obtain white matter tract segmentation.

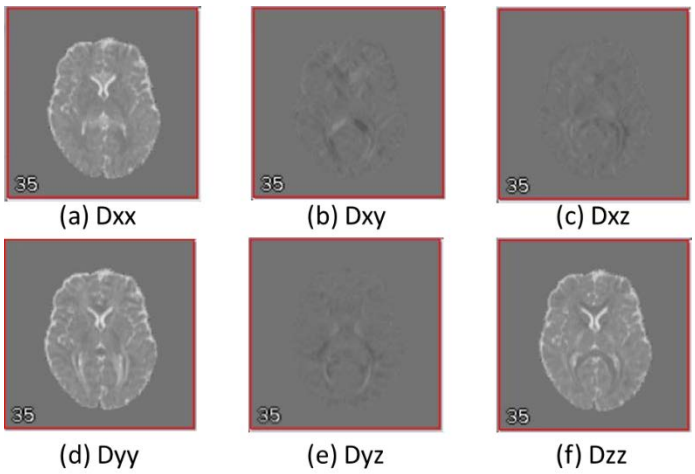

Figure 16. Tensor image estimated by DTIFIT from FSL. (a) to (f) are different directions of diffusion tensor

The Illinois Institute of Technology (IIT) Human Brain Atlas [67] consists

of anatomical, DTI, probabilistic white matter labels, and many other kinds of files. All the files are compatible with common neuroimaging tools such as FSL [67], and DTI-TK [69]. There are three kinds of registrations of the tensors: rigid, affine, and diffeomorphic. The registered tensors can then be used for calculation of DTI metrics reflecting microstructure.

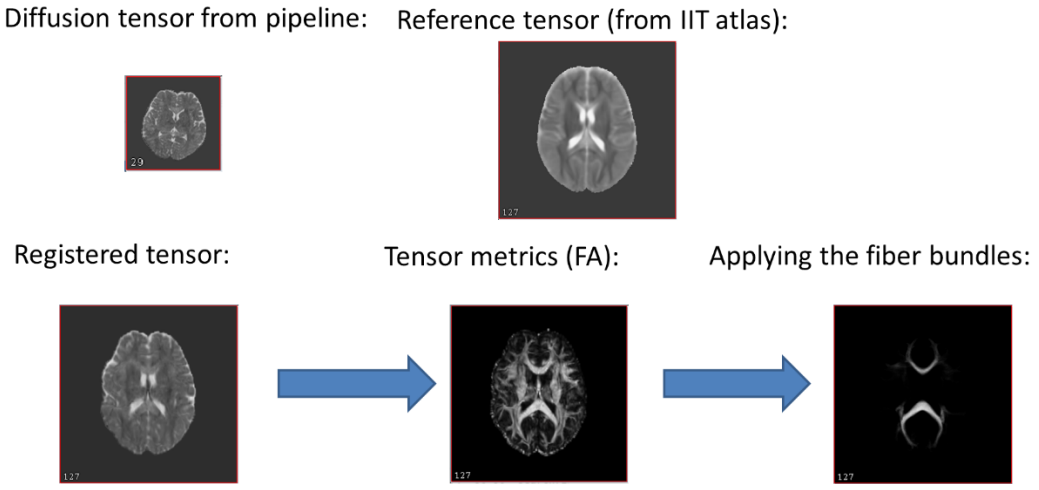

Figure 17. The steps of white matter tracts segmentation using IIT atlas.

The IIT Human Brain Atlas includes track density maps for major white matter bundles which can be converted to masks for use in region of interest analysis. After applying the masks to the registered DTI metric images, the white matter was segmented into different tracts. In the IIT human brain atlas, there are 42 labels for different white matter bundles.

Table 7. List of white matter bundles.

Label	Name
AC	anterior commissure
AF_L	left arcuate fasciculus

Label	Name
AF_R	right arcuate fasciculus
AST_L	left frontal aslant tract
AST_R	right frontal aslant tract
C_L	left cingulum
C_R	right cingulum
CC_ForcepsMajor	forceps major
CC_ForcepsMinor	forceps minor
CC	corpus callosum
CCMid	middle of corpus callosum
CST_L	left corticospinal tract
CST_R	right corticospinal tract
F_L_R	fornix
FPT_L	left frontopontine
FPT_R	right frontopontine
ICP_L	left inferior cerebellar peduncle
ICP_R	right inferior cerebellar peduncle
IFOF_L	left inferior frontooccipital fasciculus
IFOF_R	right inferior frontooccipital fasciculus
ILF_L	left inferior longitudinal fasciculus
ILF_R	right inferior longitudinal fasciculus
MCP	middle cerebellar peduncle
MdLF_L	left middle longitudinal fasciculus
MdLF_R	right middle longitudinal fasciculus
ML_L	left medial lemniscus
ML_R	right medial lemniscus
OPT_L	left occipitopontine tract
OPT_R	right occipitopontine tract
OR_L	left optic radiation
OR_R	right optic radiation
PPT_L	left parietopontine tract
PPT_R	right parietopontine tract
SCP	superior cerebellar peduncle
SLF_L	left superior longitudinal fasciculus
SLF_R	right superior longitudinal fasciculus
STT_L	left spinothalamic tract
STT_R	right spinothalamic tract
UF_L	left uncinate fasciculus

Label	Name
UF_R	right uncinate fasciculus
VOF_L	left vertical occipital fasciculus
VOF_R	right vertical occipital fasciculus

5.3 Cross-sectional Comparison

Cross-sectional comparisons of DTI parameters from different ROIs were conducted using two-way Analysis of Covariance (ANCOVA) in R [63]. Since healthy controls only have two visits with an interval of six months, Visit 1 in this part is the time point within ten days post-injury while Visit 2 is the time point six months post-injury. Data from 43 healthy controls as well as 58 patients in Visit 1 and 32 healthy controls as well as 46 patients in Visit 2 were examined. As seen in the CONSORT figure showing the flow of subjects through the trial.

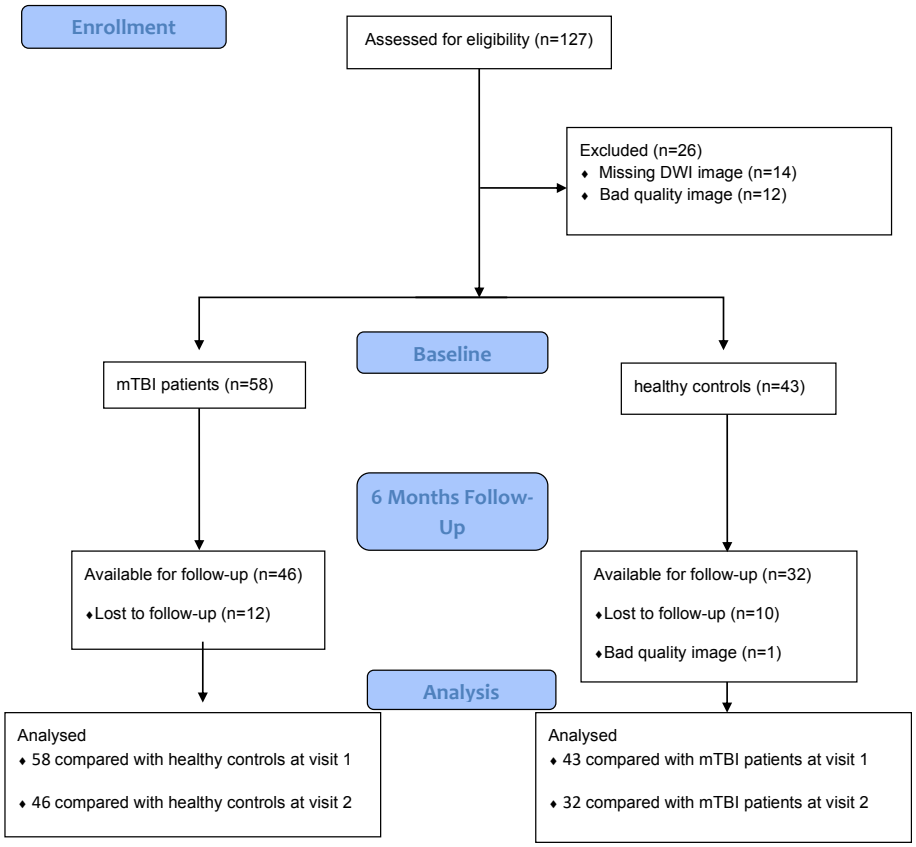

Figure 18. CONSORT figure in cross-sectional DTI metric study.

The main effects for this model are visit, group (mTBI, control), and their interactions. Age and sex are treated as covariates. The p-values were corrected for multiple comparisons.

After correcting for the covariates, no significant differences in any of the ROIs observed between the patients with mTBI and control subjects were found for FA, MD, AD, or RD for the ten day or six-month time points.

Six ROIs were selected as representatives and their results are shown in the following sections. They are corpus callosum (CC), forceps major

(CCForcepsMajor), forceps minor (CCForcepsMinor), middle of corpus callosum (CCMid), left superior longitudinal fasciculus (SLFL), and right superior longitudinal fasciculus (SLFR).

The means for groups that are adjusted for means of other factors in the model are called least square means. Least square means and their standard errors are calculated and shown in Table 8. The confidence intervals were adjusted for multiple comparisons.

Table 8. Group information after adjusted for means of other factors in the model.

ROIs	Visit	group	lsmean	SE	df	lower CL	upper CL
CC	1	HC	0.345	0.00362	158	0.336	0.355
	2	HC	0.341	0.00417	158	0.33	0.351
	1	patient	0.343	0.00359	158	0.334	0.353
	2	patient	0.341	0.00363	158	0.332	0.35
CCForcepsMajor	1	HC	0.36	0.00439	158	0.349	0.371
	2	HC	0.358	0.00506	158	0.346	0.371
	1	patient	0.353	0.00435	158	0.342	0.364
	2	patient	0.354	0.00439	158	0.343	0.365
CCForcepsMinor	1	HC	0.354	0.00471	158	0.342	0.366
	2	HC	0.349	0.00542	158	0.335	0.363
	1	patient	0.354	0.00467	158	0.342	0.365
	2	patient	0.353	0.00471	158	0.341	0.365
CCMid	1	HC	0.363	0.00417	158	0.352	0.373
	2	HC	0.357	0.0048	158	0.345	0.369
	1	patient	0.36	0.00413	158	0.349	0.37
	2	patient	0.354	0.00417	158	0.344	0.365
SLFL	1	HC	0.328	0.00383	158	0.318	0.338
	2	HC	0.323	0.00441	158	0.312	0.334
	1	patient	0.32	0.00379	158	0.31	0.329
	2	patient	0.322	0.00383	158	0.313	0.332
SLFR	1	HC	0.332	0.00358	158	0.323	0.341
	2	HC	0.33	0.00412	158	0.32	0.341
	1	patient	0.332	0.00355	158	0.323	0.341

ROIs	Visit	group	lsmean	SE	df	lower CL	upper CL
SLFR	2	patient	0.331	0.00358	158	0.321	0.34

Note. lsmean refers to least squared means, SE refers to standard error, df refers to degree of freedom, and CL refers to confidence limit.

Table 9 shows the pairwise difference and significance of FA between different groups in different visits. The p-value was corrected for multiple comparisons. Most corrected p-values are close to 1 and no significance in the pairwise comparison is shown. "1, HC" means healthy controls at Visit 1 while "2, patient" means mTBI patients at Visit 2. "1, HC-2, HC" and "1, patient-2, patient" represent within group difference over time. "1, HC-1, patient" and "2, HC-2, patient" represent between group difference at the same visit.

Table 9. Pairwise comparison of different groups.

ROIs	comparison	estimated difference	SE	df	t ratio	corrected p value
CC	1,HC-2,HC	0.00446	0.00548	158	0.814	0.848
	1,HC-1,patient	0.001927	0.00502	158	0.384	0.9807
	2,HC-2,patient	0.000277	0.00545	158	0.051	1
	1,patient-2,patient	0.002811	0.00495	158	0.568	0.9414
CCForcepsMajor	1,HC-2,HC	0.001736	0.00664	158	0.261	0.9937
	1,HC-1,patient	0.006654	0.00608	158	1.094	0.6937
	2,HC-2,patient	0.0042	0.0066	158	0.636	0.9202
	1,patient-2,patient	-0.00072	0.00599	158	-0.12	0.9994
CCForcepsMinor	1,HC-2,HC	0.005255	0.00712	158	0.738	0.8817
	1,HC-1,patient	0.000534	0.00652	158	0.082	0.9998
	2,HC-2,patient	-0.00435	0.00708	158	-0.615	0.9273
	1,patient-2,patient	0.000368	0.00643	158	0.057	0.9999
CCMid	1,HC-2,HC	0.00596	0.00631	158	0.944	0.7813
	1,HC-1,patient	0.00288	0.00578	158	0.498	0.9594
	2,HC-2,patient	0.0026	0.00627	158	0.414	0.9759
	1,patient-2,patient	0.00568	0.00569	158	0.997	0.7512

ROIs	comparison	estimated difference	SE	df	t ratio	corrected p value
SLFL	1,HC-2,HC	0.005182	0.00579	158	0.895	0.8077
	1,HC-1,patient	0.008132	0.0053	158	1.534	0.42
	2,HC-2,patient	0.000577	0.00576	158	0.1	0.9996
	1,patient-2,patient	-0.00237	0.00523	158	-0.454	0.9688
SLFR	1,HC-2,HC	1.68E-03	0.00542	158	0.31	0.9896
	1,HC-1,patient	4.27E-05	0.00496	158	0.009	1
	2,HC-2,patient	-8.46E-05	0.00539	158	-0.016	1
	1,patient-2,patient	1.55E-03	0.00489	158	0.318	0.9889

Note. "1,HC" means healthy controls at Visit 1 while "2,patient" means mTBI patients at Visit 2. SE represents standard error and df represents degree of freedom.

$*$ indicates P $\leqslant$ 0.05. $**$ indicates P $\leqslant$ 0.01. $***$ indicates P $\leqslant$ 0.001.

From Tables 8 and 9, all differences (within group and between group) are small and no significance was found.

Figure 14 shows the corresponding pairwise comparison plots with error bars. The blue lines refer to the results of healthy controls while the yellow lines refer to the results of the mTBI patients. From the results of corpus callosum, forceps major, middle of corpus callosum, left superior longitudinal fasciculus, right superior longitudinal fasciculus, the two lines are largely overlap and show no significance between mTBI patients and healthy controls for FA.

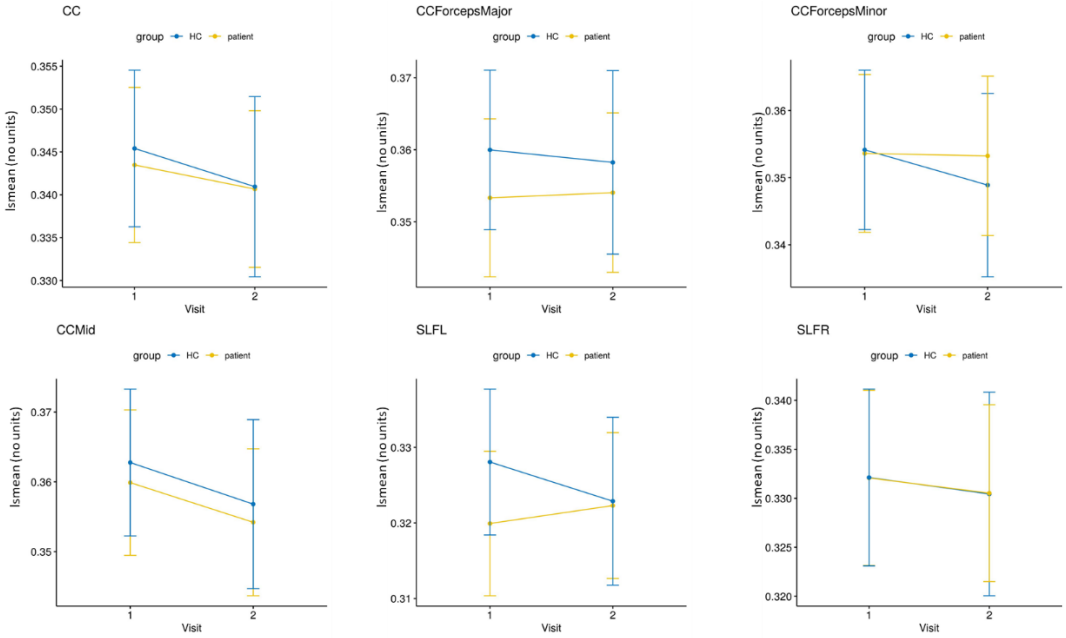

Figure 19. FA pairwise comparison plots of Corpus callosum, forceps major, forceps minor, middle CC, left and right superior longitudinal fasciculus with error bars. The error bars represent the standard error of means.

Similar results were obtained for MD, AD, and RD. Figures 20–22 show the corresponding pairwise comparison plots for corpus callosum, forceps major, forceps minor, middle CC, and left and right superior longitudinal fasciculus with error bars. The error bars represent the standard error of the least squared means. No significance was found in all these tests.

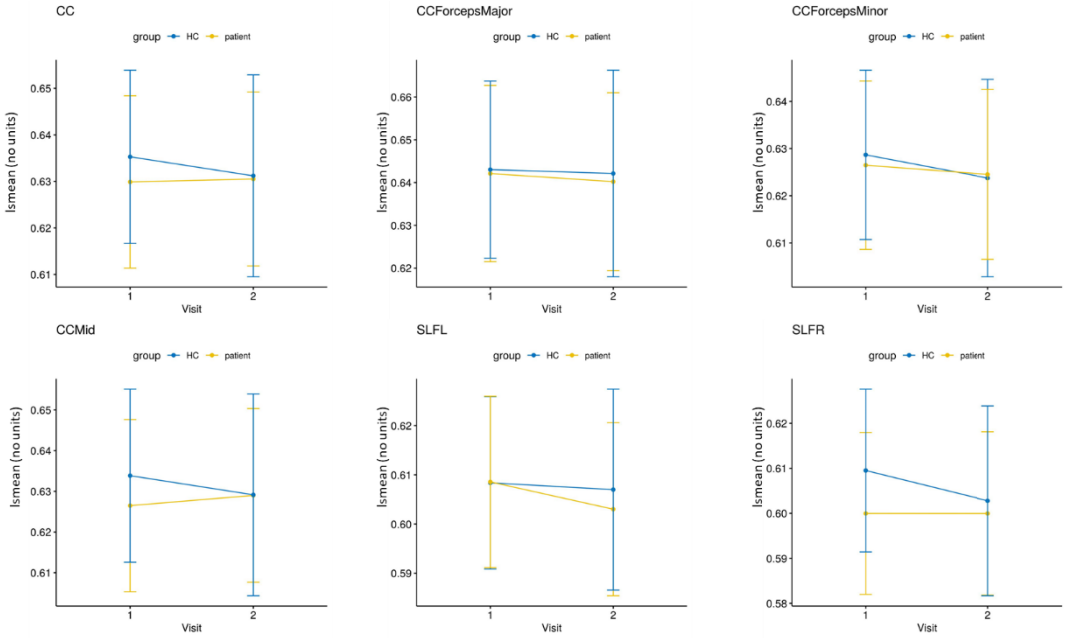

Figure 20 MD pairwise comparison plots of Corpus callosum, forceps major, forceps minor, middle CC, left and right superior longitudinal fasciculus with error bars. The error bars represent the standard error of means.

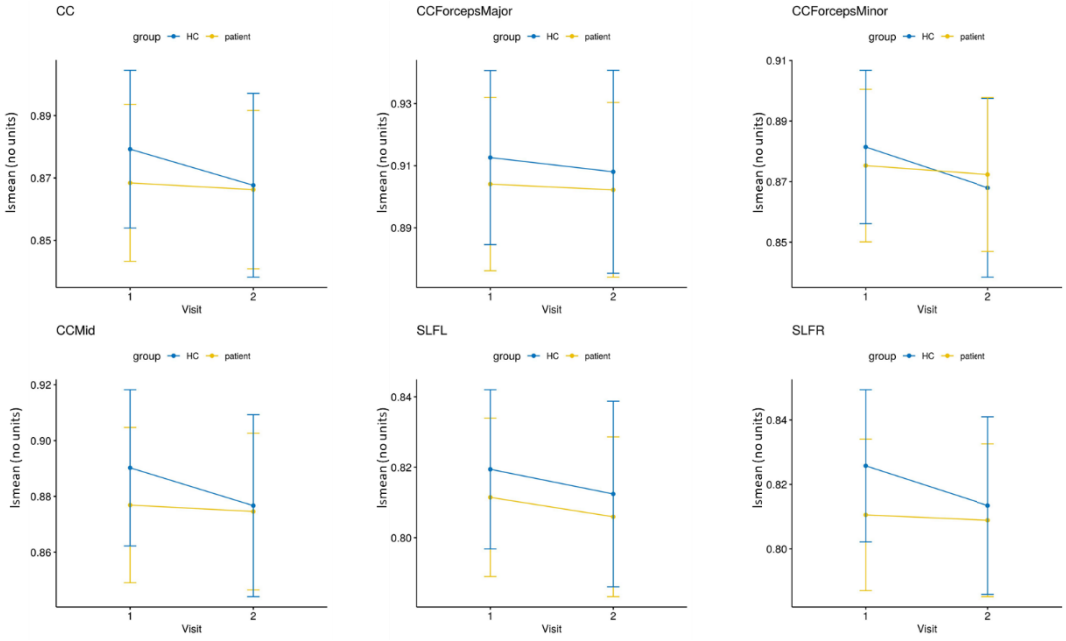

Figure 21 AD pairwise comparison plots of Corpus callosum, forceps major, forceps minor, middle CC, left and right superior longitudinal fasciculus with error bars. The error bars represent the standard error of means.

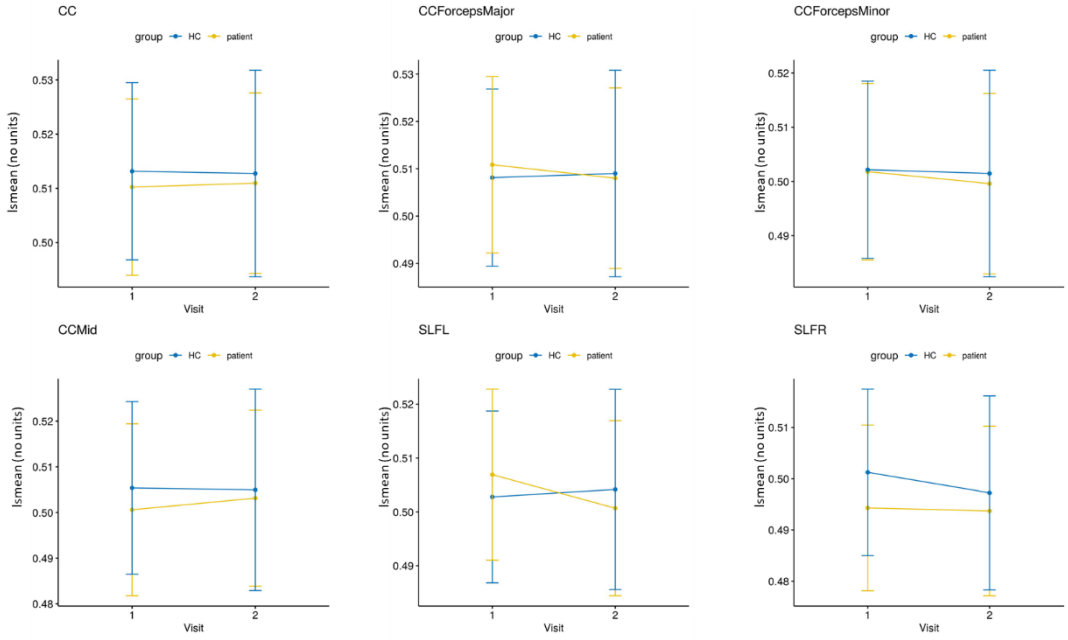

Figure 22 RD pairwise comparison plots of Corpus callosum, forceps major, forceps minor, middle CC, left and right superior longitudinal fasciculus with error bars. The error bars represent the standard error of means.

5.4 Longitudinal Comparison

Statistical tests were performed for longitudinal comparison of diffusion metrics using the linear mixed effects model in R [63]. Since some visits were missing for some of the subjects, different numbers of visits were used. In this part, there are 58 data sets for Visit 1, 55 data sets for Visit 2, 46 data sets for Visit 3, and 43 data sets for Visit 4. The linear mixed model has the advantage of dealing with missing data. Assuming the missing data is "missing at random", it uses maximum likelihood to get estimates of the parameters of the model and give unbiased results in the presence of missing data.

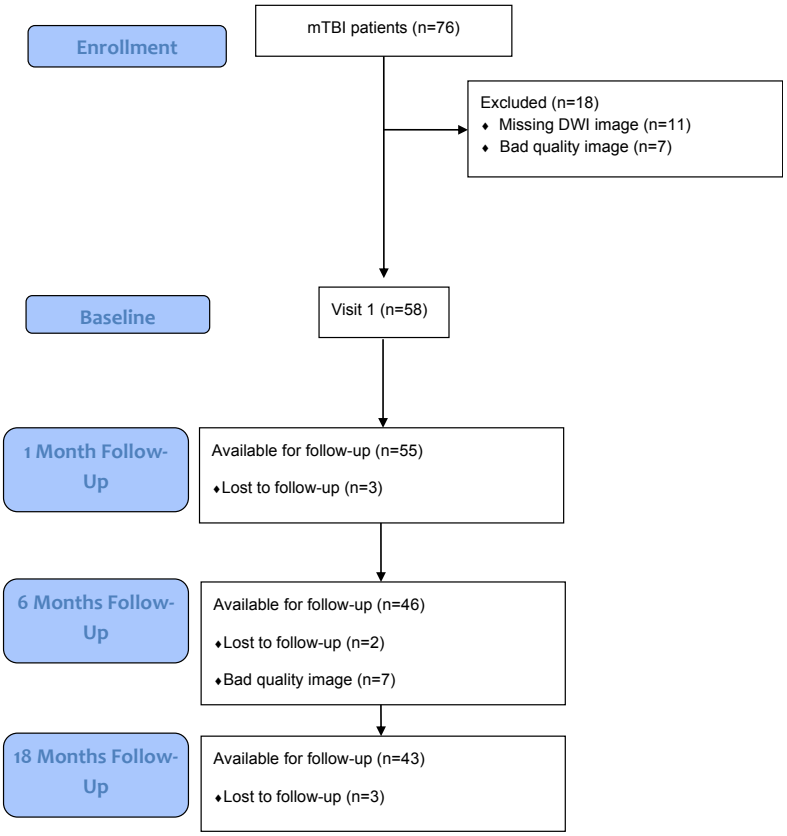

Figure 23. CONSORT figure in longitudinal DTI metric study.

It was hypothesized that mild TBI patients would show a decrease in FA and increase in MD for white matter tracts over time. This hypothesis was tested using a linear mixed effects model with the effect of visits, sex, age, interaction between ages and visits, and interaction between sex and visits being the fixed effects. Visit is the main effect we are trying to examine while sex and age are the covariates since there are known or potential effects on brain structure. The effect of ICV is not a fixed effect since the brains were registered and all the brains are of the same size in the normalized spaced.

The random effects are still an individual effect. Type I error levels were used to test whether the fixed effects are significantly different.

Since the analysis is a multiple comparison, p-value corrections were made for controlling the type I error. The Tukey method was used to prevent small p-values (below 5%) happening by chance.

No significant differences after p-value corrections in any of the ROIs were observed in mTBI patients for MD, FA, AD, or RD over the four visits.

The means for groups that are adjusted for means of other factors in the model are called least square means. Least square means and their standard errors are calculated and shown in Table 10. The confidence intervals were adjusted for multiple comparisons.

Table 10 Group information after adjusted for means of other factors in the model.

ROIs	Visit	lsmean	SE	df	lower CL	upper CL
CC	1	0.342	0.00348	83.1	0.333	0.351
	2	0.342	0.00342	78.3	0.333	0.351
	3	0.34	0.0034	76.8	0.332	0.349
	4	0.342	0.0035	84.8	0.333	0.351
CCForcepsMajor	1	0.353	0.00467	85.7	0.341	0.365
	2	0.355	0.00459	80.4	0.343	0.366
	3	0.352	0.00456	78.7	0.34	0.364
	4	0.351	0.0047	87.5	0.339	0.363
CCForcepsMinor	1	0.354	0.00409	78.2	0.343	0.364
	2	0.353	0.00403	74.5	0.343	0.363
	3	0.353	0.00402	73.2	0.343	0.363
	4	0.353	0.00411	79.5	0.343	0.364
CCMid	1	0.357	0.0041	84.6	0.346	0.367
	2	0.358	0.00402	79.6	0.347	0.368
	3	0.354	0.004	77.9	0.344	0.364

ROIs	Visit	lsmean	SE	df	lower CL	upper CL
CCMid	4	0.355	0.00412	86.4	0.345	0.366
SLFL	1	0.321	0.00353	94.4	0.312	0.33
	2	0.323	0.00345	87.5	0.314	0.332
	3	0.32	0.00342	85.3	0.312	0.329
	4	0.323	0.00356	96.8	0.314	0.332
SLFR	1	0.332	0.00355	83.9	0.323	0.341
	2	0.332	0.00349	79	0.323	0.341
	3	0.33	0.00347	77.4	0.321	0.339
	4	0.333	0.00358	85.7	0.324	0.342

Note. lsmean refer to least squared means, SE refer to standard error, df refer to degree of freedom, and CL refer to confidence limit.

Table 11 shows the pairwise difference and significance in different visits. The p-value was corrected for multiple comparisons.

Table 11. Pairwise comparison of different visits.

ROIs	comparison	estimated difference	SE	df	t ratio	corrected p value
CC	1-2	0.000218	0.00205	97	0.106	1
	1-3	0.0017	0.00212	98.2	0.803	0.9634
	1-4	0.00046	0.0023	99	0.2	1
	2-3	0.001482	0.00201	98	0.736	0.9761
	2-4	0.000242	0.00221	98.9	0.11	1
	3-4	-0.00124	0.00216	98.6	-0.575	0.9934
CCForcepsMajor	1-2	-0.00174	0.00289	97.1	-0.604	0.9914
	1-3	0.000788	0.00298	98.4	0.265	0.9999
	1-4	0.002036	0.00324	99.4	0.628	0.9894
	2-3	0.002531	0.00284	98.2	0.893	0.9399
	2-4	0.003778	0.00311	99.2	1.215	0.787
	3-4	0.001247	0.00304	98.9	0.411	0.999
CCForcepsMinor	1-2	5.72E-04	0.00216	96.8	0.266	0.9999
	1-3	6.68E-04	0.00223	97.7	0.3	0.9998
	1-4	6.33E-04	0.00242	98.4	0.261	0.9999
	2-3	9.52E-05	0.00212	97.5	0.045	1

ROIs	comparison	estimated difference	SE	df	t ratio	corrected p value
CCForcepsMinor	2-4	6.05E-05	0.00232	98.2	0.026	1
	3-4	-3.47E-05	0.00227	98	-0.015	1
CCMid	1-2	-0.00099	0.00248	97	-0.4	0.9991
	1-3	0.002844	0.00257	98.3	1.109	0.849
	1-4	0.001138	0.00279	99.3	0.408	0.999
	2-3	0.003838	0.00244	98.2	1.573	0.5325
	2-4	0.002132	0.00268	99.1	0.797	0.9648
	3-4	-0.00171	0.00262	98.7	-0.652	0.9871
SLFL	1-2	-0.00187	0.00249	97.5	-0.754	0.9732
	1-3	0.000763	0.00256	99.3	0.298	0.9998
	1-4	-0.00171	0.00279	100.7	-0.615	0.9906
	2-3	0.002637	0.00244	99.1	1.081	0.8635
	2-4	0.000162	0.00267	100.4	0.061	1
	3-4	-0.00248	0.00261	99.9	-0.947	0.9216
SLFR	1-2	-0.00036	0.00213	97	-0.167	1
	1-3	0.00208	0.0022	98.2	0.947	0.9216
	1-4	-0.00092	0.00239	99.2	-0.384	0.9993
	2-3	0.002436	0.00209	98.1	1.166	0.8168
	2-4	-0.00056	0.00229	99	-0.245	0.9999
	3-4	-0.003	0.00224	98.7	-1.339	0.7043

Note. "1-2" means comparison between Visit 1 and Visit 2. SE represents standard error and df represents degree of freedom.

$*$ indicates $P \leqslant 0.05$. $**$ indicates $P \leqslant 0.01$. $***$ indicates $P \leqslant 0.001$.

Figure 18 shows the pairwise comparison plots for FA with means and error bars for the corpus callosum, forceps major, middle of corpus callosum, left superior longitudinal fasciculus, and right superior longitudinal fasciculus. The lines indicate the changing trend of each ROIs. From Figure 18, no trends can be observed from the lines and the results show no significant difference in FA between mTBI patients and healthy controls.

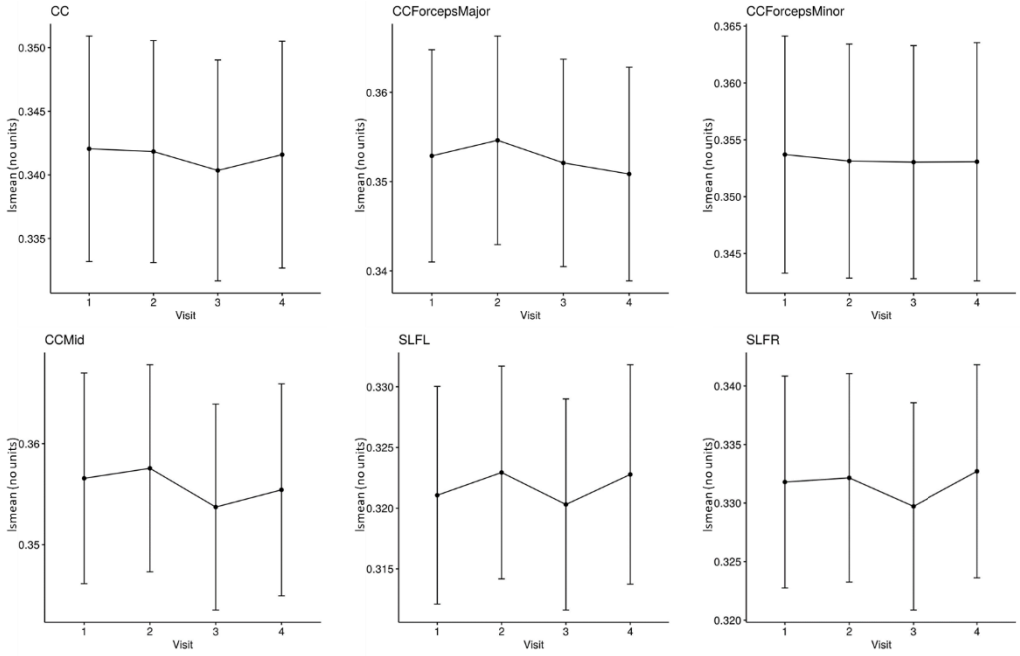

Figure 24. Least squared means of Corpus callosum, forceps major, forceps minor, middle CC, left and right superior longitudinal fasciculus with error bars over four visits regarding FA. The unit of y-axis is mm³. The error bars represent the standard error of least squared means.

Similar results were obtained for MD, AD, and RD. Figures 25–27 show the corresponding pairwise comparison plots for the corpus callosum, forceps major, forceps minor, middle CC, and left and right superior longitudinal fasciculus. The error bars on these plots represent the standard error of the least squared means. Although in Visit 4, the least square means are shown to be higher than the former visit, no significance was found in any of these tests.

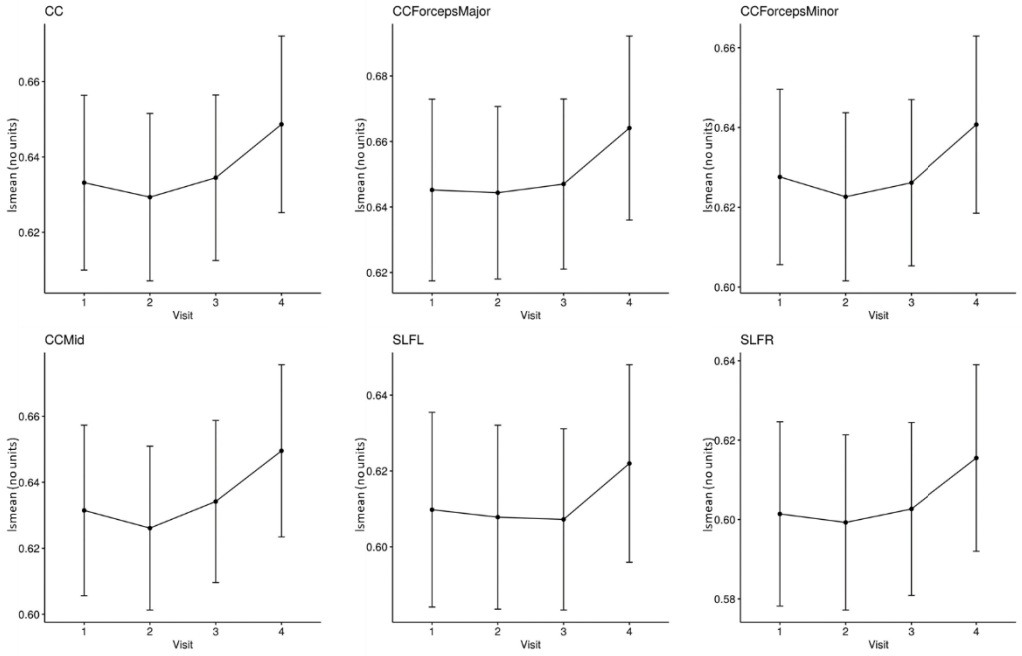

Figure 25. Least squared means of Corpus callosum, forceps major, forceps minor, middle CC, left and right superior longitudinal fasciculus with error bars over four visits regarding MD. The unit of y-axis is mm³. The error bars represent the standard error of least squared means.

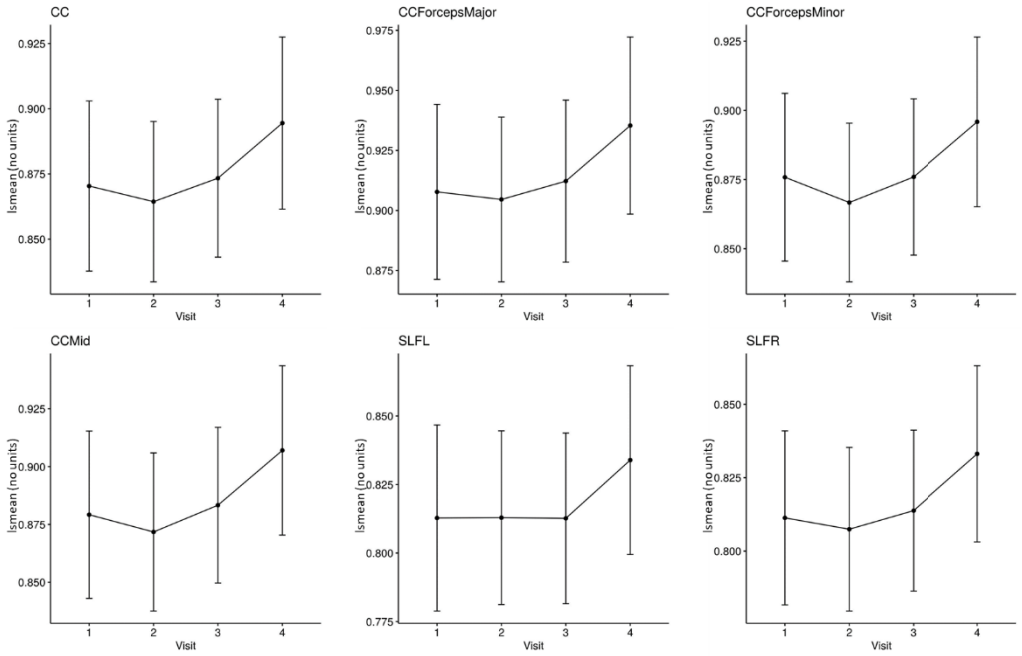

Figure 26. Least squared means of Corpus callosum, forceps major, forceps minor, middle CC, left and right superior longitudinal fasciculus with error bars over four visits regarding MD. The unit of y-axis is mm³. The error bars represent the standard error of least squared means.

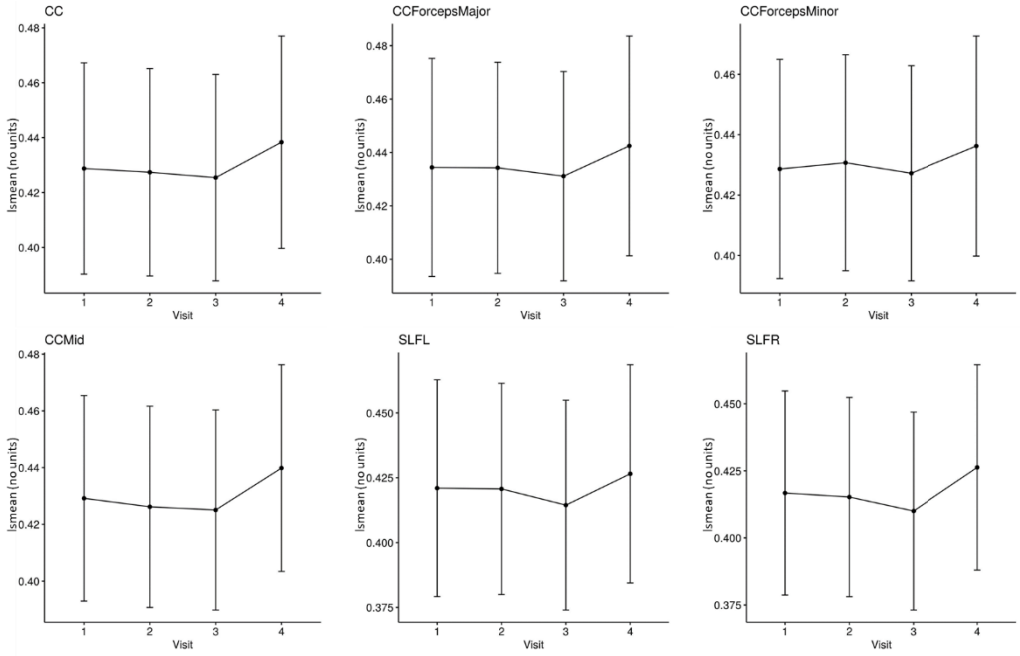

Figure 27. Least squared means of Corpus callosum, forceps major, forceps minor, middle CC, left and right superior longitudinal fasciculus with error bars over four visits regarding MD. The unit of y-axis is mm³. The error bars represent the standard error of least squared means.

Although no significant changes were found from the results of the corpus callosum, forceps major, forceps minor, middle CC, and left and right superior longitudinal fasciculus, it is worth mentioning that on Visit 4, there are sudden increases in MD, AD, and RD. The increase in the six ROIs is not shown in the FA results. Although the increases are not significant, they show potential increasing trends in MD, AD, and RD in the six areas over 18 months.

Chapter 6 Conclusion and Discussion

In this study, brain changes in mild TBI patients were examined. Both regional volume changes and DTI parameters were employed to show how the brain might be affected by mild TBI in comparison to healthy controls.

In volumetric analysis, it was hypothesized that mild TBI patients would show a decrease in WM as well as GM volumes while an increase in CSF volume compared with healthy controls. It was also hypothesized that mild TBI patients would show a decrease in white matter volume and gray matter volume while showing increase in ventricular CSF over time. A cross-sectional comparison of patients and healthy controls and a longitudinal comparison were conducted in this study to verify the hypotheses.

From the results of cross-sectional volume study, no significant results were found in GM, WM, and CSF. However, some areas of GM, i.e., the right

fusiform gyrus, right postcentral gyrus medial segment, left postcentral gyrus medial segment, left posterior insula, left superior frontal gyrus, and right transverse temporal gyrus, were found to have significant difference between the mTBI group and healthy controls. Most of the differences were observed on the second visit, i.e. six months after injury. However, those regions are small gray matter structures and the significant difference was not found in their contralateral counterparts. In that case, six months may not be enough to observe significant changes in regional brain volumes. Future work could examine the cross-sectional differences between mild TBI patients and healthy controls over a longer time period or can consider the same analysis in more severe TBI patients.

In the longitudinal study comparing regional volumes, nine regions were found to have significant changes over time for mTBI patients. Those regions can be divided into two groups: gray matter labels and ventricular CSF labels. The left lateral ventricle, 3rd ventricle, and ventricular CSF belong to the CSF group and they show an increasing trend over the four visits. The left accumbens area, right amygdala, left ventral diencephalon, left frontal operculum, left frontal operculum, right occipital fusiform gyrus, left planum temporale, and right temporal pole belong to the gray matter group and a decreasing trend was observed in those regions over the four visits. The trends agree with the hypothesis that gray matter volume would decrease

while CSF volume would increase longitudinally in mild TBI patients. However, the decreasing trend was only found in some of the gray matter areas and no significant regional volume changes over time in the cerebral WM, GM, or VBP were found.

In DTI metrics analysis, it was hypothesized that mild TBI patients would show decreased FA, increased MD, decreased AD, and increased RD compared to healthy controls. It was also hypothesized that the mTBI patients would show more decreased FA, increased MD, decreased AD, and increased RD over time. A Cross-sectional comparison of patients and healthy controls and a longitudinal comparison were conducted in this study to verify the hypotheses.

Analyses of FA, MD, AD, and RD from the DTI images do not show significant diffusion changes over time in patients compared to healthy controls. If there are changes, they may be too small for our study to observe and either more subjects or more sensitive methods would be necessary to reveal them.

Besides DTI images, there are also many longitudinal studies of DKI images in mild TBI. Grossman et al. [70][71] conducted DKI longitudinal studies of mild TBI patients and examined changes in the thalamus. Stokum et al. [16] used DKI metrics mean kurtosis (MK) and radial kurtosis (Kr) and found out reduced Kr and MK in the anterior internal capsule and reduced

MK in the posterior internal capsule in mild TBI patients over six months post-injury while the DTI parameters remained unchanged. It was therefore suggested that measurements of MK and Kr can help lead to a better understanding of the physiological changes of mild TBI.

DKI metrics also show superiority over DTI metrics in other studies. In a study of brain maturation, Falangola et al. [72] have shown that MK is sensitive to changes in GM and WM, where MK increases with brain maturation while the DTI parameters, MD and FA remained relatively unchanged. They concluded that diffusional kurtosis is able to characterize and measure age-related diffusion changes for both grey and white matter, in the developing and aging brain.

Dependence only on DTI parameters may underestimate the underlying cellular processes that influence changes in the tissue microstructure [73]. Zhuo et al. [73] studied changes in DTI parameters and DKI parameters in several white and gray matter regions in a mild controlled cortical impact (CCI) injury rat model at both the acute (2 h) and the sub-acute (7 days) stages following injury. An increase in MK at the sub-acute stage was observed in the contralateral regions compared to baseline while no change was observed with MD and FA. The results suggest that DKI is sensitive to microstructural changes which may be underestimated by standard DTI parameters alone. MK changes provide information of molecular and

morphological changes in vivo and may act as complementary information in addition to changes in standard DTI parameters.

The study also indicates that changes in diffusion kurtosis parameters correspond to active processes that involve reactive astrocytes not realized by DTI [73]. Since reactive astrogliosis is considered to be a reliable and sensitive biomarker for insults from traumatic brain injury and it can play an important role in determining the clinical outcome, the use of DTI has been limited to study changes in white matter integrity following traumatic insults. In that case, with the sensitivity to detect microstructural changes even in the gray matter in vivo, DKI allows the extension of the technique to understand patho-morphological changes in the whole brain following a traumatic insult.

In addition, Phillips et al. [74] and Filippi et al. [75] have shown tractography's potential for identifying structural connectivity changes occurring between the acute and chronic stages of traumatic brain injury and for predicting patients' long-term outcome. Future works could be made to incorporate the fiber tracking results for longitudinal study of white matter tracts connectivity in mild TBI patients.

Bibliography

1 National Hospital Discharge Survey (NHDS), 2010; National Hospital Ambulatory Medical Care Survey (NHAMCS), 2010; public use data file: CDC National Center for Health Statistics. Available at: https://www.cdc.gov/traumaticbraininjury/index.html. Accessed 15 Mar 2020.

2 Thurman, D. J., Alverson, C., Dunn, K. A., Guerrero, J., and Sniezek, J. E. "Traumatic brain injury in the United States: a public health perspective." The Journal of Head Trauma Rehabilitation, 14(6): 602-615, 1999.

3 Taylor, C. A., Bell, J. M., Breiding, M. J., and Xu, L. "Traumatic brain injury–related emergency department visits, hospitalizations, and deaths—United States, 2007 and 2013." MMWR Surveillance

Summaries, 66(9): 1, 2017

4 Marin, J. R., Weaver, M. D., Yealy, D. M., and Mannix, R. C. "Trends in visits for traumatic brain injury to emergency departments in the United States." The Journal of the American Medical Association, 311(18): 1917-1919, 2014.

5 Ruff, R. M., Iverson, G. L., Barth, J. T., Bush, S. S., Broshek, D. K., and NAN Policy and Planning Committee. "Recommendations for diagnosing a mild traumatic brain injury: a National Academy of Neuropsychology education paper." Archives of Clinical Neuropsychology, 24(1): 3-10, 2009.

6 Setnik, L., and Bazarian, J. J. "The characteristics of patients who do not seek medical treatment for traumatic brain injury." Brain Injury, 21(1): 1-9, 2007.

7 Silverberg, N. D., Duhaime, A. C., and Iaccarino, M. A. "Mild Traumatic Brain Injury in 2019-2020." The Journal of the American Medical Association, 323(2): 177-178, 2020.

8 Gioia, G. A., Collins, M., and Isquith, P. K. "Improving identification and diagnosis of mild traumatic brain injury with evidence: psychometric support for the acute concussion evaluation." The Journal of Head Trauma Rehabilitation, 23(4): 230-242, 2008.

9 Matis, G., and Birbilis, T. "The Glasgow Coma Scale–a brief review Past, present, future." Acta Neurologica Belgica, 108(3): 75-89, 2008.

10 Narayana, P. A. "White matter changes in patients with mild traumatic brain injury: MRI perspective." Concussion, 2(2): CNC35, 2017.

11 Gale, S. D. "White matter pathway degeneration following traumatic brain injury: Morphometric and neuropsychologic correlates." Unpublished dissertation. Brigham Young University, Provo, Utah, 1994.

12 Sidaros, A., Engberg, A. W., Sidaros, K., Liptrot, M. G., Herning, M., Petersen, P., Paulson, O.B., Jernigan, T.L., and Rostrup, E. "Diffusion tensor imaging during recovery from severe traumatic brain injury and relation to clinical outcome: a longitudinal study." Brain, 131(2): 559-572, 2008.

13 Bendlin, B. B., Ries, M. L., Lazar, M., Alexander, A. L., Dempsey, R. J., Rowley, H. A., Sherman, J.E., and Johnson, S. C. "Longitudinal changes in patients with traumatic brain injury assessed with diffusion-tensor and volumetric imaging." NeuroImage, 42(2): 503-514, 2008.

14 Betz, J., Zhuo, J., Roy, A., Shanmuganathan, K., and Gullapalli, R. P. "Prognostic value of diffusion tensor imaging parameters in severe traumatic brain injury." Journal of Neurotrauma, 29(7): 1292-1305, 2012.

15 Zhou, Y., Milham, M. P., Lui, Y. W., Miles, L., Reaume, J., Sodickson, D. K., Grossman, R.I., and Ge, Y. "Default-mode network disruption in mild traumatic brain injury." Radiology, 265(3): 882-892, 2012.

16 Stokum, J. A., Sours, C., Zhuo, J., Kane, R., Shanmuganathan, K., and Gullapalli, R. P. "A longitudinal evaluation of diffusion kurtosis imaging in patients with mild traumatic brain injury." Brain Injury, 29(1): 47-57, 2015.

17 Zhou, Y., Kierans, A., Kenul, D., Ge, Y., Rath, J., Reaume, J., Grossman, R.I., and Lui, Y. W. "Mild traumatic brain injury: longitudinal regional brain volume changes." Radiology, 267(3): 880-890, 2013.

18 Anderson, C. V., and Bigler, E. D. "The role of caudate nucleus and corpus callosum atrophy in trauma-induced anterior horn dilation." Brain Injury, 8(6): 565-569, 1994

19 Anderson, C. V., Wood, D. M. G., Bigler, E. D., and Blatter, D. D.

"Lesion volume, injury severity, and thalamic integrity following head injury." Journal of Neurotrauma, 13(2): 59-65, 1996

20 Bigler, E. D., Blatter, D. D., Anderson, C. V., Johnson, S. C., Gale, S. D., Hopkins, R. O., and Burnett, B. "Hippocampal volume in normal aging and traumatic brain injury." American Journal of Neuroradiology, 18(1): 11-23, 1997.

21 Gale, S. D., Burr, R. B., Bigler, E. D., and Blatter, D. "Fornix degeneration and memory in traumatic brain injury." Brain Research Bulletin, 32(4): 345-349, 1993.

22 Yount, R., Raschke, K. A., Biru, M., Tate, D. F., Miller, M. J., Abildskov, T., Gandhi, P., Ryser, D. Hopkins, R.O., and Bigler, E. D. "Traumatic brain injury and atrophy of the cingulate gyrus." The Journal of Neuropsychiatry and Clinical Neurosciences, 14(4): 416-423, 2002.

23 Raz, E., Jensen, J. H., Ge, Y., Babb, J. S., Miles, L., Reaume, J., Grossman, R.I. and Inglese, M. "Brain iron quantification in mild traumatic brain injury: a magnetic field correlation study." American Journal of Neuroradiology, 32(10): 1851-1856, 2011.

24 Tang, L., Ge, Y., Sodickson, D. K., Miles, L., Zhou, Y., Reaume, J., and Grossman, R. I. "Thalamic resting-state functional networks:

disruption in patients with mild traumatic brain injury." Radiology, 260(3): 831-840, 2011.

25 Prasad, A. "Making images/making bodies: Visibilizing and disciplining through magnetic resonance imaging (MRI)." Science, Technology, and Human Values, 30(2): 291-316, 2005.

26 Brown, M. A., Semelka, R. C., and Dale, B. M. "MRI: Basic Principles and Applications. " John Wiley and Sons, 2011.

27 Steyn, J. H., and Smith, F. W. "Nuclear magnetic resonance imaging of the prostate." British Journal of Urology, 54(6): 726-728, 1982.

28 McRobbie, D. W., Moore, E. A., Graves, M. J., and Prince, M. R. "MRI from Picture to Proton. " Cambridge University Press, 2017.

29 Wang, J., He, L., Zheng, H., and Lu, Z. L. "Optimizing the magnetization-prepared rapid gradient-echo (MP-RAGE) sequence. " PloS One, 9(5): 2014.

30 Mugler J. P., Brookeman J. R. Three-dimensional magnetization-prepared rapid gradient-echo imaging (3D MP RAGE). Magnetic Resonance in Medicine, 15: 152–157.

31 Brant-Zawadzki, M., Gillan, G. D., and Nitz, W. R. "MP RAGE: a three-dimensional, T1-weighted, gradient-echo sequence--initial experience in the brain. " Radiology, 182(3): 769-775, 1992.

32 Kecskemeti, S., Samsonov, A., Hurley, S. A., Dean, D. C., Field, A., and Alexander, A. L. "MPnRAGE: A technique to simultaneously acquire hundreds of differently contrasted MPRAGE images with applications to quantitative T1 mapping. " Magnetic Resonance in Medicine, 75(3): 1040-1053, 2016.

33 Ashburner, J., and Friston, K. J. "Voxel-based morphometry—the methods. " NeuroImage, 11(6): 805-821, 2000.

34 Sastre-Garriga, J., Arévalo, M. J., Renom, M., Alonso, J., González, I., Galán, I., Montalban, X. and Rovira, A. "Brain volumetry counterparts of cognitive impairment in patients with multiple sclerosis. " Journal of the Neurological Sciences, 282(1-2): 120-124, 2009.

35 Briellmann, R. S., Pell, G. S., Wellard, R. M., Mitchell, L. A., Abbott, D. F., and Jackson, G. D. "MR imaging of epilepsy: State of the art at 1.5 T and potential of 3 T. " Epileptic Disorders, 5(1): 3-20, 2003.

36 Le Bihan, D., Mangin, J. F., Poupon, C., Clark, C. A., Pappata, S., Molko, N., and Chabriat, H. "Diffusion tensor imaging: concepts and applications." Journal of Magnetic Resonance Imaging, 13(4): 534-546, 2001.

37 Huisman, T. A. "Diffusion-weighted imaging: basic concepts and application in cerebral stroke and head trauma." European Radiology, 13(10): 2283-2297, 2003.

38 Beaulieu, C. "The basis of anisotropic water diffusion in the nervous system–a technical review." NMR in Biomedicine, 15(7-8): 435-455, 2002.

39 Hagmann, P., Thiran, J. P., Jonasson, L., Vandergheynst, P., Clarke, S., Maeder, P., & Meuli, R. "DTI mapping of human brain connectivity: statistical fibre tracking and virtual dissection." NeuroImage, 19(3): 545-554, 2003.

40 Le Bihan, D., Mangin, J. F., Poupon, C., Clark, C. A., Pappata, S., Molko, N., & Chabriat, H. "Diffusion tensor imaging: concepts and applications." Journal of Magnetic Resonance Imaging, 13(4): 534-546, 2001.

41 Mukherji, S. K., Chenevert, T. L., and Castillo, M. "Diffusion-weighted magnetic resonance imaging." Journal of Neuro-ophthalmology, 22(2): 118-122, 2002.

42 Dietrich, O., Biffar, A., Baur-Melnyk, A., and Reiser, M. F. "Technical aspects of MR diffusion imaging of the body." European Journal of Radiology, 76(3): 314-322, 2010.

43 Srinivasan, A., Goyal, M., Azri, F. A., and Lum, C. "State-of-the-art imaging of acute stroke." Radiographics, 26: S75-S95, 2006.

44 Kubicki, M., Westin, C. F., McCARLEY, R. W., and Shenton, M. E. "The application of DTI to investigate white matter abnormalities in schizophrenia." Annals of the New York Academy of Sciences, 1064: 134, 2005.

45 Basser, P. J., Mattiello, J., Turner, R., and Le Bihan, D. "Diffusion tensor echo-planar imaging of human brain." Proceedings of the ISMRM, 584, 1993.

46 Basser, P. J. "Inferring microstructural features and the physiological state of tissues from diffusion-weighted images." NMR in Biomedicine, 8(7): 333-344, 1995.

47 Alexander, A. L., Lee, J. E., Lazar, M., and Field, A. S. "An introduction to diffusion tensor image analysis." Neurosurgery, 22(2): 185-196, 2011.

48 Alexander, A. L., Lee, J. E., Lazar, M., and Field, A. S. "Diffusion tensor imaging of the brain." Neurotherapeutics, 4(3): 316-329, 2007.

49 Löbel, U., Sedlacik, J., Güllmar, D., Kaiser, W. A., Reichenbach, J. R., and Mentzel, H. J. "Diffusion tensor imaging: the normal evolution of ADC, RA, FA, and eigenvalues studied in multiple

anatomical regions of the brain." Neuroradiology, 51(4): 253-263, 2009.

50 Colby, J. B., Soderberg, L., Lebel, C., Dinov, I. D., Thompson, P. M., and Sowell, E. R. "Along-tract statistics allow for enhanced tractography analysis." NeuroImage, 59(4): 3227-3242, 2012.

51 Muftuler, L. T. "Quantifying Morphology and Physiology of the Human Body using MRI. " CRC Press, 2013.

52 Madden, D. J., Bennett, I. J., Burzynska, A., Potter, G. G., Chen, N. K., and Song, A. W. "Diffusion tensor imaging of cerebral white matter integrity in cognitive aging." Biochimica et Biophysica Acta (BBA)-Molecular Basis of Disease, 1822(3): 386-400, 2012.

53 Barrio-Arranz, G., de Luis-Garcia, R., Tristán-Vega, A., Martin-Fernandez, M., and Aja-Fernández, S. "Impact of MR acquisition parameters on DTI scalar indexes: a tractography based approach." PloS One, 10(10), 2015.

54 Liu, X., Yang, Y., Sun, J., Yu, G., Xu, J., Niu, C., Tian, H., and Lin, P. "Reproducibility of diffusion tensor imaging in normal subjects: an evaluation of different gradient sampling schemes and registration algorithm." Neuroradiology, 56(6): 497-510, 2014.

55 Jensen, J. H., and Helpern, J. A. "MRI quantification of

non-Gaussian water diffusion by kurtosis analysis. " NMR in Biomedicine, 23(7): 698-710, 2010.

56 Fieremans, E., Jensen, J. H., and Helpern, J. A. "White matter characterization with diffusional kurtosis imaging. " NeuroImage, 58(1): 177-188, 2011.

57 DeCarlo, L. T. "On the meaning and use of kurtosis. " Psychological Methods, 2(3): 292, 1997.

58 Marrale, M., Collura, G., Brai, M., Toschi, N., Midiri, F., La Tona, G., Lo Casto, A, and Gagliardo, C. "Physics, techniques and review of neuroradiological applications of diffusion kurtosis imaging (DKI)." Clinical Neuroradiology, 26(4): 391-403, 2016.

59 Zhu, J., Zhuo, C., Qin, W., Wang, D., Ma, X., Zhou, Y., and Yu, C. "Performances of diffusion kurtosis imaging and diffusion tensor imaging in detecting white matter abnormality in schizophrenia." NeuroImage: Clinical, 7: 170-176, 2015.

60 Tustison N.J., Avants B.B., Cook P.A., Zheng Y., Egan A., Yushkevich P.A. and Gee J.C.: "N4ITK: improved N3 bias correction. " IEEE Trans Med Imaging, 2010.

61 Koval, V., Farmaga, I. W., Strojwas, A. J., and Director, S. W. "MONSTR: A complete thermal simulator of electronic systems."

Proceedings of the 31st Annual Design Automation Conference. 1994.

62 Huo, Y., Carass, A., Resnick, S. M., Pham, D. L., Prince, J. L., and Landman, B. A. "Combining multi-atlas segmentation with brain surface estimation." SPIE Medical Imaging, International Society for Optics and Photonics, 97840E-997848, 2016.

63 R Core Team. "R: A language and environment for statistical computing." Vienna: R Foundation for Statistical Computing, 2013.

64 "Longitudinal Study". En.Wikipedia.Org, 2020, Available at: https://en.wikipedia.org/wiki/Longitudinal_study. Accessed 15 Mar 2020.

65 West, B. T., Welch, K. B., and Galecki, A. T "Linear mixed models: a practical guide using statistical software. " CRC Press, 2014.

66 Taris, T. W. "A primer in Longitudinal Data Analysis. " Sage, 2000.

67 M. Jenkinson, C.F. Beckmann, T.E. Behrens, M.W. Woolrich, S.M. Smith. "FSL." NeuroImage, 62:782-90, 2012

68 Zhang, S., and Arfanakis, K. "Evaluation of standardized and study-specific diffusion tensor imaging templates of the adult human brain: Template characteristics, spatial normalization accuracy, and detection of small inter-group FA differences." NeuroImage, 172: 40-

50, 2018.

69 Wang, Y., Gupta, A., Liu, Z., Zhang, H., Escolar, M. L., Gilmore, J. H., Gouttard, S., Fillard, P., Maltbie, E. Gerig, G, and Styner, M. "DTI registration in atlas based fiber analysis of infantile Krabbe disease." NeuroImage, 55(4): 1577-1586, 2011.

70 Grossman, E. J., Ge, Y., Jensen, J. H., Babb, J. S., Miles, L., Reaume, J., Silver, J.M., Grossman, R.I. and Inglese, M. "Thalamus and cognitive impairment in mild traumatic brain injury: A diffusional kurtosis imaging study." Journal of Neurotrauma, 29:2318–2327, 2012.

71 Grossman, E. J., Jensen, J. H., Babb, J. S., Chen, Q., Tabesh, A., Fieremans, E., Xia, D., Inglese, M., and Grossman, R. I. "Cognitive impairment in mild traumatic brain injury: A longitudinal diffusional kurtosis and perfusion imaging study." American Journal of Neuroradiology, 34(5), 951-957, 2013.

72 Falangola, M. F., Jensen, J. H., Babb, J. S., Hu, C., Castellanos, F. X., Di Martino, A., Ferris, S. H., and Helpern, J. A. "Age-related non-Gaussian diffusion patterns in the prefrontal brain." Journal of Magnetic Resonance Imaging: An Official Journal of the International Society for Magnetic Resonance in Medicine, 28(6): 1345-1350, 2008.

73 Zhuo, J., Xu, S., Proctor, J. L., Mullins, R. J., Simon, J. Z., Fiskum, G., and Gullapalli, R. P. "Diffusion kurtosis as an in vivo imaging marker for reactive astrogliosis in traumatic brain injury." NeuroImage, 59(1): 467-477, 2012.

74 Phillips, O., Sanchez-Castaneda, C., Elifani, F., Maglione, V., Di Pardo, A., Caltagirone, C., Squitieri, F., Sabatini, U., and Di Paola, M. "Tractography of the corpus callosum in Huntington's disease." PloS One, 8: e73280, 2013.

75 Filippi, M., and Agosta, F. "Diffusion tensor imaging and functional MRI." Handbook of clinical neurology. 136: 1065-1087, 2016.

Vita

Zhongyan Xiong

Tel: (+1)4434537830 E-mail: zxiong6@jhu.edu

Linkedin: linkedin.com/in/zhongyan-xiong

EDUCATION

Johns Hopkins University **Baltimore, MD**

Master of Engineering in Biomedical Engineering *Aug. 2018 – May. 2020*

- **Focus area:** Imaging & Medical Devices
- **Courses:** Machine Learning for Signal Processing, Principles of Design of BME Instrumentation, Computer Integrated Surgery I, Medical Imaging System, Introduction to Data Science for Biomedical Engineering, Medical Image Analysis, Introduction to Neuro-Image Processing

Zhejiang University (Chu Kochen Honors College) **Hangzhou, China**

Bachelor of Engineering in Biomedical Engineering (Overall GPA: 3.87 /4.00) *Sept. 2014- Jun. 2018*

- **Honors:** Scholarship for Outstanding Merits, Excellent Student Award
- **Courses:** Probability Theory, C programming, Circuit and Electronic Technology, Linear Algebra

SKILLS

- Programming Languages: C/C++, SQL, JAVA, Python, R, MATLAB, Linux
- Platforms: Android, PyTorch, Keras, Microsoft Office
- Algorithms: Machine learning, UNET
- Image Processing Methods and Signal Processing

WORK EXPERIENCE

The First Affiliated Hospital of Zhejiang University **Hangzhou, China**

department of instrumentation *Jan. 2018-Feb. 2018*

- Quality inspection of instruments like ear thermometer, electrocardiogram monitor, etc.
- Learned the operation of CT, ultrasound machine through technical tours.
- Observed surgeries conducted by surgical robot and learned the basic operation.
- Assist engineers in instrument maintenance and paperwork.

TECHNICAL RESEARCH

Longitudinal Analysis of Patients with Mild Traumatic Brain Injury **Baltimore, MD**

Instructor: Prof. Jerry Prince *Jan. 2020-May.2020*

- Whole brain segmentation using multi-atlas segmentation and white matter tract segmentation using IIT atlas segmentation.
- Evaluated regional changes in mild TBI patients over 16 months.
- Evaluated group difference on regional changes of mild Traumatic Brain Injury (TBI) patients compared to healthy controls.
- Assessed with regional volumes and diffusion tensor imaging (DTI) parameters.
- Designed two-way ANCOVA and linear mixed effect models in cross-sectional and longitudinal analysis.

Brain Fiber Orientation Reconstruction using Deep Learning Network **Baltimore, MD**

Instructor: Prof. Jerry Prince & Prof. Chuyang Ye *Jun. 2019-Sept. 2019*

- Preprocessed diffusion tensor images(DTI) and extracted diffusion metrics such as mean diffusivity (MD), fractional anisotropy (FA), deterministic fiber tracking tensors.
- Synthesized diffusion signals with a single-tensor or multi-tensor model using basis tensors for each voxel.
- Estimated the mixture fractions of the dictionary atoms using feed forward deep network, while ensuring that the mixed fractional vectors are sparsely distributed, ie, only three directions at most in a voxel.
- Compare with other state-of-art methods and evaluate the proposed method.

Mammography abnormality detection and diagnosis **Baltimore, MD**

Instructor: Prof. Jerry Prince *Feb. 2019-May. 2019*

- Presented a Computer-aided diagnosis (CAD) model for Mammography abnormality detection and diagnosis, which is composed of preprocessing, breast density classification, abnormality diagnosis, segmentation of masses, and benignity and malignancy diagnosis.
- Used region growing method and contrast limited adaptive histogram equalization for pectoral muscle removal and image enhancement. Extracted morphological and texture features for classification and detection.
- Evaluated the model using confusion matrices, speed, sensitivity and specificity.

ECG-based Identity Recognition via PCA **Baltimore, MD**

Instructor: Prof. Nitish Thakor *Nov. 2018*

- Established an ECG-based biosecurity interface. Applied PCA algorithm to extract features from ECG signals and identify the host of the ECG signals. Evaluated the performance of the algorithm.

Design of immunosensors for reproductive hormone **Hangzhou, China**

Instructor: Prof. Qingjun Liu *Mar. 2017-Jun. 2018*

- Designed immunosensors for reproductive hormones such as human chorionic gonadotropin (hCG) and luteinizing hormone (LH), using nanomaterials such as AuNPs, MoS2 and GR-PBA composite.
- Studied the corresponding antigen-antibody response. Gained certain knowledge of different character of different nanomaterials.

Design of electrochemical biosensors with peptide probes **Hangzhou, China**

Instructor: Prof. Qingjun Liu *Jul. 2016-Apr. 2017*

- Designed a sensitive biosensor based on the electrochemical detection and analyzed the specific target molecule reaction on the peptide molecule. Detected linoleic acid and oleic acid with immobile human ordorant binding protein (hOBP) on it.
- Gained a certain understanding of process of designing an electrochemical biosensor and had a grasp of using electrochemical workstation.